THE JOURNAL OF BIOLOGICAL CHEMISTRY VOL. 290, NO. 38, pp. 23094–23109, September 18, 2015

Probing the Catalytic Mechanism of Copper Amine Oxidase from *Arthrobacter globiformis* with Halide Ions*

Received for publication, May 1, 2015, and in revised form, August 11, 2015 Published, JBC Papers in Press, August 11, 2015, DOI 10.1074/jbc.M115.662726

Takeshi Murakawa[‡], Akio Hamaguchi[§], Shota Nakanishi[§], Misumi Kataoka[¶‖], Tadashi Nakai[§], Yoshiaki Kawano[‖], Hiroshi Yamaguchi[¶‖], Hideyuki Hayashi[**], Katsuyuki Tanizawa[§‡‡], and Toshihide Okajima[§1]**

From the [‡]Department of Biochemistry, Osaka Medical College, Takatsuki, Osaka 569-8686, Japan, the [§]Institute of Scientific and Industrial Research, Osaka University, Ibaraki, Osaka 567-0047, Japan, the [¶]School of Science and Technology, Kwansei Gakuin University, Sanda, Hyogo 669-1337, Japan, the [‖]Advanced Photon Technology Division, RIKEN SPring-8 Center, Sayo-gun, Hyogo 679-5148, Japan, the [**]Department of Chemistry, Osaka Medical College, Takatsuki, Osaka 569-8686, Japan, and the [‡‡]Center of the Region Haná for Biotechnological and Agricultural Research, Faculty of Science, Palacký University, 783 71 Olomouc, Czech Republic

Background: Copper amine oxidases catalyze amine oxidation using copper and a quinone cofactor.
Results: Halides bind axially to the copper center, preventing the reduced cofactor from adopting an on-copper conformation.
Conclusion: The cofactor undergoes large conformational changes during the catalytic reaction that enable transitions between different types of chemistry.
Significance: Molecular details of cofactor movement have been unveiled based on structural and kinetic evidence.

The catalytic reaction of copper amine oxidase proceeds through a ping-pong mechanism comprising two half-reactions. In the initial half-reaction, the substrate amine reduces the Tyr-derived cofactor, topa quinone (TPQ), to an aminoresorcinol form (TPQ_{amr}) that is in equilibrium with a semiquinone radical (TPQ_{sq}) via an intramolecular electron transfer to the active-site copper. We have analyzed this reductive half-reaction in crystals of the copper amine oxidase from *Arthrobacter globiformis*. Anerobic soaking of the crystals with an amine substrate shifted the equilibrium toward TPQ_{sq} in an "on-copper" conformation, in which the 4-OH group ligated axially to the copper center, which was probably reduced to Cu(I). When the crystals were soaked with substrate in the presence of halide ions, which act as uncompetitive and noncompetitive inhibitors with respect to the amine substrate and dioxygen, respectively, the equilibrium in the crystals shifted toward the "off-copper" conformation of TPQ_{amr}. The halide ion was bound to the axial position of the copper center, thereby preventing TPQ_{amr} from adopting the on-copper conformation. Furthermore, transient kinetic analyses in the presence of viscogen (glycerol) revealed that only the rate constant in the step of TPQ_{amr}/TPQ_{sq} interconversion is markedly affected by the viscogen, which probably perturbs the conformational change. These findings unequivocally demonstrate that TPQ undergoes large conformational changes during the reductive half-reaction.

Copper amine oxidases (CAOs[2]; EC 1.4.3.6) catalyze the oxidative deamination of various primary amines to produce the corresponding aldehydes and ammonia, coupled with the reduction of molecular oxygen to hydrogen peroxide (1–3). CAOs play distinct physiological roles in prokaryotes and eukaryotes. Prokaryotic CAOs mainly function to assimilate primary amines as carbon and nitrogen sources for growth. Eukaryotic CAOs have versatile functions, being involved in the detoxification of bio-active amines, such as histamine (4); cell adhesion (5); cell death (6); collagen cross-linking in animals (7); and germination, root growth, and healing of wounded cell walls in plants (8). It has been reported that human serum CAOs cause angiopathy in diabetes (9). Therefore, various CAO inhibitors have been developed as therapeutic drugs (10, 11).

The catalytic center common to the CAO family consists of a mononuclear copper ion and a redox-active organic cofactor, topa quinone (TPQ), which is generated through posttranslational and self-catalytic processes (12–15). As summarized in a recent review (3), x-ray crystal structures of CAOs have been determined for a number of enzymes from various sources, including bacteria (*Escherichia coli* (16) and *Arthrobacter globiformis* (AGAO) (17–19)), yeasts (*Hansenula polymorpha* (recently reclassified as *Pichia angusta*) (HPAO-1 and HPAO-2) (20, 21) and *Pichia pastoris* (lysyl oxidase) (22)), a

* This work was supported by Japan Society for the Promotion of Science Grants-in-Aid for Scientific Research 23770127 and 26440037 (to T. M.) and 18350085 and 15K07391 (to T. O.); Operational Program Education for Competitiveness-European Social Fund Project CZ.1.07/2.3.00/20.0165) (to K. T.); and by funding from the Network Joint Research Center for Materials and Devices. The authors declare that they have no conflicts of interest with the contents of this article.

The atomic coordinates and structure factors (codes 3X3X, 3X3Y, 3X3Z, 3X40, 3X41, and 3X42) have been deposited in the Protein Data Bank (http://wwpdb.org/).

[1] To whom correspondence should be addressed: Institute of Scientific and Industrial Research, Osaka University, Ibaraki, Osaka 567-0047, Japan. Tel.: 81-6-6879-4292; Fax: 81-6-6879-8464; E-mail: tokajima@sanken.osaka-u.ac.jp.

[2] The abbreviations used are: CAO, copper amine oxidase; AGAO and HPAO, CAO from *A. globiformis* and *H. polymorpha*, respectively; 2-PEA, 2-phenylethylamine; TPQ, topa quinone; TPQ_{imq}, iminoquinone form of TPQ; TPQ_{psb}, product Schiff base of TPQ; TPQ_{ssb}, substrate Schiff base of TPQ; TPQ_{ox}, oxidized form of TPQ; TPQ_{amr}, reduced (aminoresorcinol) form of TPQ; TPQ_{sq}, semiquinone radical form of TPQ; TAPS, 3-{[2-hydroxy-1,1-bis(hydroxymethyl)ethyl]amino}-1-propanesulfonic acid; CHES, 2-(cyclohexylamino)ethanesulfonic acid; PAA, phenylacetaldehyde.

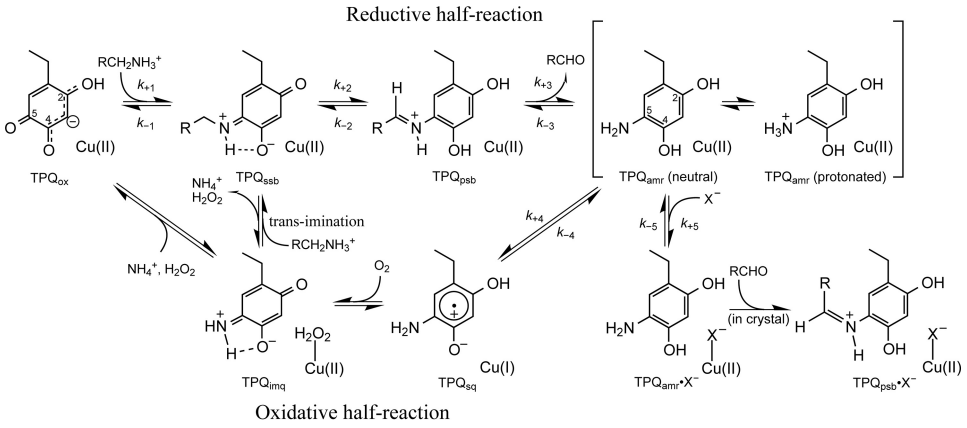

SCHEME 1. **Presumed catalytic mechanism of AGAO.**

fungus (*Aspergillus nidulans* (23)), a plant (*Pisum savitum* (24)), a mammal (*Bos taurus* (25)), and *Homo sapiens* (diamine oxidase and vascular adhesion protein 1, which is identical to semicarbazide-sensitive amine oxidase (26–28)). The active site structures of these enzymes, including the positions of TPQ and Cu(II), are highly conserved, suggesting that they have a common mechanism for single-turnover TPQ biogenesis and catalytic amine oxidation. The latter process has been shown to proceed through a ping-pong mechanism consisting of two half-reactions (Scheme 1) (1–3).

In the initial reductive half-reaction, the C5 carbonyl group of the oxidized cofactor (TPQ_{ox}) undergoes nucleophilic attack by amine substrate to form the substrate Schiff base (TPQ_{ssb}). Stereospecific proton abstraction by a conserved base (Asp-298 in AGAO) (29) converts TPQ_{ssb} to the product Schiff base (TPQ_{psb}). Concomitantly with the release of the corresponding aldehyde, TPQ_{psb} is hydrolyzed to the reduced cofactor (an aminoresorcinol form, TPQ_{amr}) that is in equilibrium with a semiquinone radical form (TPQ_{sq}) via the single electron transfer reduction of Cu(II) to Cu(I). In these steps of the reductive half-reaction, the cofactor ring is not directly ligated to the copper atom (a configuration designated the "off-copper" conformation), whereas in the TPQ_{sq}·Cu(I) state, the cofactor ring is assumed to be directed toward the metal in the so-called "on-copper" conformation to facilitate electron transfer. This suggests that the equilibrium between TPQ_{amr}·Cu(II) and TPQ_{sq}·Cu(I) is accompanied by a substantial conformational reorganization of the TPQ ring. Indeed, the conformational flexibility of TPQ within the active site of CAOs has previously been suggested to be important in catalysis (24, 30, 31). In the subsequent oxidative half-reaction, the reduced cofactor is reoxidized by dioxygen to produce hydrogen peroxide and an iminoquinone intermediate (TPQ_{imq}), which is further hydrolyzed to form the oxidized cofactor, releasing ammonia in the following step (1–3). In the presence of excess substrate, it is assumed that TPQ_{imq} reacts directly with the substrate amine to form TPQ_{ssb} (via a *trans*-imination reaction) rather than regenerating TPQ_{ox} (Scheme 1).

Depending on the enzyme sources and reaction conditions, such as pH and temperature, various amounts of TPQ_{sq}·Cu(I) are known to be formed by adding an amine substrate under anaerobic conditions, which is assumed to induce the reductive half-reaction. However, the mechanistic role of the TPQ_{sq}·Cu(I) form in the subsequent O_2 reduction remains unclear and controversial (32–39). Two reaction pathways for the O_2 reduction have been proposed, depending on the enzyme sources. One is an inner sphere mechanism in which O_2 is coordinated on Cu(I) and reduced by the transfer of two electrons from TPQ_{sq}·Cu(I) to ultimately produce a Cu(II)-bound peroxide species and TPQ_{imq} (Scheme 1). The necessary singlet to triplet spin transition is allowed by the coordination of O_2 to Cu(I). AGAO and *P. savitum* CAO are CAOs that have been suggested to follow this mechanism (37, 38). The formation of the TPQ_{sq}·Cu(I) state at the beginning of the oxidative half-reaction is believed to be essential in this process. The other mechanism that has been proposed is an outer sphere process that is suggested to occur in bovine serum CAO (34) and HPAO-1 (36, 39). In both of these enzymes, O_2 binds to a hydrophobic pocket close to the cofactor and is initially reduced by TPQ_{amr} via a single electron transfer that does not change the oxidation state of the Cu(II) center. The resulting superoxide anion then coordinates to Cu(II), inducing the second electron transfer. The TPQ_{sq}·Cu(I) complex is not formed in this catalytic cycle and is assumed to be an off-pathway product generated only by the anaerobic reduction of the CAO by the amine substrate.

We have previously determined x-ray crystal structures of the intermediates, including TPQ_{ssb} and TPQ_{psb}, formed during the reductive half-reaction of AGAO with 2-phenylethylamine (2-PEA) (29), tyramine (40), and ethylamine (41). In each case, the TPQ cofactor in these structures had an off-copper conformation. Here, we present new high resolution structures of TPQ_{sq} formed in the reductive half-reaction of AGAO with 2-PEA and histamine. The TPQ_{sq} formed with these substrates exists exclusively in the on-copper conformation with the 4-OH group ligating axially to the copper center, which is probably in the Cu(I) oxidation state. Moreover, we found that the off-copper TPQ_{amr} is formed when the crystals are soaked with substrate in the presence of halide ions that act as uncompetitive inhibitors with respect to the amine substrate and noncompetitive inhibitors with respect to dioxygen. Halide ions bind axially to the copper center, preventing TPQ_{amr} from coordinating to copper. Combined with the results of spectrophotometric, steady-state, and transient kinetics analyses, the results presented herein provide unequivocal evidence for the occur-

rence of a large conformational change in the TPQ cofactor during the reductive half-reaction of AGAO.

Experimental Procedures

Materials—Recombinant AGAO was purified as its inactive precursor and converted to the copper- and TPQ-containing active form as reported previously (12, 19). Protein and TPQ_{sq} concentrations were determined spectrophotometrically using molar extinction coefficients of $\epsilon_{280} = 93{,}200\ \text{M}^{-1}\ \text{cm}^{-1}$ (12) and $\epsilon_{468} = 4500\ \text{M}^{-1}\ \text{cm}^{-1}$, respectively (35). All amine substrates used for kinetic analyses and crystal soaking were neutralized with 1 M H_2SO_4.

Spectrophotometric Measurements—To achieve fully anaerobic conditions, the enzyme and substrate solutions were kept in a vacuum-type glove box (Iuchi, SGV-65V) filled with 99.999% (v/v) argon gas for at least 2 h, as described previously (18). The enzyme (final concentration, 100 μM monomer) was anaerobically mixed with 1 mM 2-PEA in 50 mM HEPES, pH 6.8, in the presence or absence of various concentrations of sodium, potassium, or ammonium salts of halide ions. For measurements of pH dependence, the enzyme (100 μM monomer) was reduced with substrate in 100 mM MES (pH 5.7, 5.8, 6.0, 6.3, 6.5, and 6.7), 100 mM HEPES (pH 7.0, 7.3, 7.5, 7.8, and 8.0), 100 mM TAPS (pH 8.5 and 9.0), or 100 mM CHES (pH 9.5 and 10.1) at a nearly constant ionic strength ($I = 0.35 \pm 0.03$) after adjustment with 100 mM Na_2SO_4. The enzyme was mixed with its substrate under anaerobic conditions in a quartz cuvette with a gas-tight screw cap, and after 5 min, the absorption spectrum was measured at 25 °C with an Agilent 8453 photodiode array spectrophotometer. An apparent pK_a value for the absorbance change at 468 nm was determined by fitting the data to Equation 1,

$$y = C_1/(1 + [H^+]/K_{a1}) + C_2/(1 + [H^+]/K_{a2}) \qquad \text{(Eq. 1)}$$

where y represents the absorbance at a particular pH, C_1 and C_2 are the pH-independent values of the absorbance, and K_{a1} and K_{a2} are the acid dissociation constants associated with the pH profile. Data fitting was performed by nonlinear regression using Kaleidagraph version 4.1 (Abelbeck Software).

Steady-state Kinetic Analysis—Steady-state kinetic analyses were conducted at 30 °C with 2-PEA, histamine, or ethylamine (hydrochloride) as the substrate using the colorimetric assay protocol described previously (12). Inhibition by halide ions was studied using assay solutions containing 2–40 μM 2-PEA and 0–50 mM NaF, NaCl, NaBr, or NaI. Inhibition constants (K_i) were determined on the basis of uncompetitive inhibition (42) with respect to the amine substrate using Equation 2,

$$v_0 = k_{cat}[S]/(K_m + (1 + [I]/K_i)[S]) \qquad \text{(Eq. 2)}$$

where v_0 represents the initial reaction rate and [S] and [I] are the concentrations of substrate and inhibitor, respectively. Data fitting was performed by multiple regression analysis using R (available from the R Project Web site). Inhibition by halide ions was also studied using assay solutions containing 8.8–1160 μM dissolved oxygen and a fixed concentration (40 μM) of 2-PEA in the presence of 0–25 mM NaCl. Various concentrations of dissolved oxygen were established by mixing 99.99% (v/v) O_2 and 99.99% (v/v) N_2 gas with a gas mixer (KOFLOC, PMG-1) and bubbling the resulting mixture through a needle into the reaction mixture contained in a tightly sealed cuvette with a silicon rubber cap. The mixed gas line was also branched into the cell of a Clark-type oxygen electrode (YSI Inc., model 5300) for determination of the dissolved oxygen concentration. The reaction was initiated by adding a small amount of the anaerobic enzyme solution with a microsyringe. Inhibition constants (K_i) were determined on the basis of noncompetitive inhibition (42) with respect to dissolved oxygen using Equation 3,

$$v_0 = k_{cat}[S]/((K_m + [S])(1 + [I]K_i)) \qquad \text{(Eq. 3)}$$

where v_0 represents the initial reaction rate, and [S] and [I] are the concentrations of dissolved oxygen and inhibitor, respectively. Data fitting was performed by multiple regression analysis using R.

The effect of solvent viscosity was investigated by measuring the enzyme's activity toward 2-PEA at 4 °C in a solution of 0–30% (w/v) glycerol or sucrose as a viscogen; the solvent's viscosity was determined relative to a buffer-only solution with an Ostwald viscometer.

Stopped-flow Measurements—Transient kinetic analyses were done at 4 °C with an Applied Photophysics stopped-flow spectrophotometer (40, 41). Typically, equal volumes (about 30 μl each) of enzyme (200 μM monomer in 50 mM HEPES buffer, pH 6.8) and substrate (1 mM 2-PEA) solutions were mixed in a 20-μl mixing cell by triggering with an N_2 gas piston; the mixing dead time was generally 2.3 ms at an N_2 gas pressure of 500 kilopascals. To avoid spectral changes associated with the oxidative half-reaction, both enzyme and substrate solutions were maintained under fully anaerobic conditions as described above. The substrate solution was supplemented with 200 mM NaCl, 600 mM NaBr, or 600 mM Na_2SO_4, as appropriate. The effect of solvent viscosity on transient kinetics was also studied as described above by adding a viscogen (0–30% (w/v) glycerol or sucrose) to both the enzyme and substrate solutions. UV-visible absorption spectra were recorded every 2.5 ms at wavelengths of 250–800 nm. Spectral data were analyzed using Pro-Kineticist II (Applied Photophysics) to obtain the spectra of the reaction intermediates and to calculate the rate constants for each reaction step.

Single-crystal Microspectrophotometry—AGAO crystals prepared as described below were subjected to microspectrophotometry before x-ray diffraction as reported previously (29).

X-ray Crystallographic Analysis—AGAO was crystallized by microdialysis essentially according to the method described previously (29). Briefly, a 15 mg/ml protein solution was dialyzed in a 50-μl dialysis button at 16 °C against 1.05 M potassium-sodium tartrate in 25 mM HEPES buffer, pH 6.8. After 2 weeks of crystal growth, the dialysis buttons were transferred into a fresh reservoir solution supplemented with 45% (v/v) glycerol as a cryoprotectant, and the crystals were soaked at 16 °C for 24 h, followed by further soaking in the fully anaerobic reservoir solution containing 45% (v/v) glycerol for 24 h. The crystals were then incubated in a solution (pH 6.8) containing 4 mM 2-PEA, 10 mM histamine, or 50 mM ethylamine (hydrochlo-

ride) with or without 100 mM NaCl or 300 mM NaBr for about 1 h until their color faded. They were then mounted on thin nylon loops (ϕ, 0.5–0.7 mm) and frozen by flash cooling in liquid CF_4. All procedures were done in the anaerobic box, and the frozen crystals were kept in liquid N_2 until x-ray diffraction analysis.

Diffraction data sets were collected at 100 K with synchrotron X-radiation using a DIP6040 imaging plate (Bruker AXS, Billerica, MA) in the BL44XU station or using a Quantum 210 CCD detector (ADSC) in the BL38B1 station at SPring-8 (Hyogo, Japan). X-rays with a wavelength of 0.919 Å were used to detect anomalous peaks derived from bromine; a wavelength of 0.9 Å was used otherwise. The collected data sets were processed and scaled using HKL2000 (43) or MOSFLM (44) and SCALA (45), respectively. The starting model was obtained by molecular replacement with Phaser (46). The search model was based on the coordinates of the AGAO monomer (Protein Data Bank code 1IU7) after removing all water molecules and a metal ion. Refinements, electron density map calculations, and assignment of solvent molecules were initially done using Refmac 5 (47) and later with Phenix (48). Manual rebuilding was performed using Coot (49), and water molecules and other ligands, such as metal ions, were added step by step to the model during the refinement process. The models of the catalytic intermediates of TPQ and phenylacetaldehyde were built using the Monomer library sketcher from the CCP4 package (50), and then the dictionary files used with Refmac 5, Phenix, and Coot were generated using the PRODRG server (51). PyMOL version 1.5 (Schrödinger, LLC) was used for figure drawings. Anomalous maps for bromine atoms were generated using fft (52) from the CCP4 package (50) based on anomalous difference and phase data for the final model. Details and statistics pertaining to the data collection and refinement are summarized in Table 1.

Results

Effect of Halide Ions on the Absorption Spectrum of TPQ_{sq}—It is well established that the absorption spectrum of the bound cofactor TPQ changes rapidly during the reductive half-reaction of CAOs (1–3), as demonstrated by stopped-flow spectrophotometry of the reaction with AGAO (29, 40, 53). The final form of TPQ in the reductive half-reaction without turnover (measured under anaerobic conditions) is TPQ_{sq}, which exhibits characteristic absorption maxima at about 440 and 470 nm with a shoulder at about 350 nm. We incidentally noted that the TPQ_{sq} spectrum of AGAO was markedly depressed in the presence of NaCl, which was added to the reaction mixture to maintain a constant ionic strength. For example, in the presence of 10 mM NaCl, the intensities of the absorption bands at 352, 438, and 468 nm decreased to about 32% of those without NaCl (Fig. 1). When calculated using the molar extinction coefficient at 468 nm ($\epsilon_{468} = 4500\ M^{-1}\ cm^{-1}$) reported for TPQ_{sq} (35), the presence of NaCl reduced the calculated TPQ content relative to total AGAO from 38 to 9.8%. This was attributed to a shift of the equilibrium between TPQ_{amr} and TPQ_{sq} (see Scheme 1) toward the former, which has no absorption bands above 300 nm (54). To identify the chemical species that caused this equilibrium shift, we investigated the effects of adding 10 mM NH_4Cl, KCl, Na_2SO_4, or NaH_2PO_4 in the reductive half-reaction and found that comparable shifts were induced by NH_4Cl and KCl but not Na_2SO_4 or NaH_2PO_4 (Fig. 1), clearly indicating that the Cl^- ion was preventing the formation of TPQ_{sq}. Other halide ions (F^-, Br^-, and I^-) behaved similarly (Fig. 2), and their effects were roughly concentration-dependent, with an order of effectiveness of $Cl^- \approx Br^- > F^- > I^-$. A similar effect (bleaching of TPQ_{sq} absorption) by a high concentration of Cl^- (0.45 M KCl) was reported in an early study on methylamine oxidase from *Arthrobacter* P1 (55), but the mechanism of bleaching was not further pursued.

Effect of Halide Ions on Catalytic Activity—We have briefly reported the inhibition of AGAO activity by Cl^- ion (56) in the past. In this work, more precise steady-state kinetic analyses were conducted by systematically varying the concentrations of the substrate amine (2-PEA) or dissolved oxygen in the presence of 0–50 mM solutions of different halide ions. Double reciprocal plots ($1/v$ *versus* $1/s$) revealed that the Cl^- ion was an uncompetitive inhibitor with respect to the substrate amine and a noncompetitive inhibitor with respect to dissolved oxygen (Fig. 3); other halide ions (F^-, Br^-, and I^-) exhibited similar inhibition patterns (data not shown). These results show that halide ions bind to a substrate·enzyme complex but not to the free enzyme and that they bind equally to the O_2-bound and O_2-unbound enzyme forms at a site distinct from the O_2-binding site (41). The K_i values calculated for uncompetitive inhibition were 97.2 ± 6.5 mM for F^-, 26.2 ± 1.4 mM for Cl^-, 58.2 ± 2.8 mM for Br^-, and 69.6 ± 9.4 mM for I^-, whereas that for noncompetitive inhibition by Cl^- was 32.8 ± 1.7 mM. The inhibition of catalytic activity by halide ions may be unique to AGAO; the Cl^- ion reportedly has no inhibitory effect on the activities of human kidney diamine oxidase, *P. pastoris* amine oxidase, or *P. savitum* CAO (57).

Effects of Halide Ions on Transient Kinetics—To identify the substrate·enzyme complex to which the halides bind, we performed transient kinetic analyses of the reductive half-reaction in the presence of 100 mM NaCl, 300 mM NaBr, or 300 mM Na_2SO_4 (as a control for the ionic strength). As reported previously (29, 40, 53), rapid spectral changes associated with changes in the redox and chemical state of TPQ ($TPQ_{ox} \rightarrow TPQ_{ssb} \rightarrow TPQ_{psb} \rightarrow TPQ_{amr} \rightarrow TPQ_{sq}$) were observed (Fig. 4). We noted that in the presence of 100 mM NaCl or 300 mM NaBr, the TPQ_{sq} absorption band appeared transiently within ~117 ms and then gradually declined in intensity to about 30–40% of the value achieved in the absence of halide ions or in the presence of 300 mM Na_2SO_4 (Fig. 4, *A* and *B*). The final spectra (at 1023 ms) acquired in the presence of NaCl or NaBr (Fig. 4, *C* and *D*) mostly lacked the TPQ_{sq}-characteristic peaks, suggesting a shift of the equilibrium toward TPQ_{amr}, as discussed above (Fig. 2, *B* and *C*).

Initially, the multiwavelength data of all spectral changes were fitted to the four-step mechanism connecting TPQ_{ox}, TPQ_{ssb}, TPQ_{psb}, TPQ_{amr}, and TPQ_{sq} (Scheme 1) by global analysis as reported previously (29). The spectral changes in the presence of 300 mM Na_2SO_4 (Fig. 4*B*) were solved to provide rate constants that were essentially identical to those obtained without the salt (Fig. 4*A*) (Table 2), and the deduced UV-visible absorption spectra (Fig. 4, *E* and *F*) of TPQ_{ox}, TPQ_{ssb}, TPQ_{psb},

TABLE 1
Data collection and crystallographic refinement statistics

	$AGAO_{PEA}$	$AGAO_{HTA}$	$AGAO_{ETA/HCl}$	$AGAO_{PEA/NaBr}$	$AGAO_{PEA/NaCl}$	$AGAO_{NaBr}$
Soaking conditions	4 mM 2-PEA, anaerobic	10 mM histamine, anaerobic	50 mM ethylamine-HCl, anaerobic	4 mM 2-PEA, 300 mM NaBr, anaerobic	4 mM 2-PEA, 100 mM NaCl, anaerobic	300 mM NaBr, aerobic
Protein Data Bank code	3X3X	3X3Y	3X3Z	3X41	3X40	3X42
Data collection						
Temperature (K)	100	100	100	100	100	100
Wavelength (Å)	0.9	0.9	0.9	0.919	0.9	0.919
Space group	*C2*	*C2*	*C2*	*C2*	*C2*	*C2*
Unit-cell dimensions						
a, *b*, *c* (Å)	191.66, 62.89, 158.01	193.47, 63.25, 157.91	192.55, 62.73, 157.65	191.62, 63.29, 157.85	191.81, 63.02, 158.11	192.68, 63.51, 158.10
β (degrees)	117.48	117.73	117.62	117.21	117.29	117.55
Resolution limit (Å)	38.5–1.57 (1.65–1.57)	50.0–1.50 (1.53–1.50)	38.5–1.51 (1.59–1.51)	47.3–1.87 (1.97–1.87)	26.5–1.85 (1.95–1.85)	100–1.89 (1.96–1.89)
No. of observations	1,511,400	1,700,730	1,862,064	503,626	520,004	935,217
No. of unique reflections	228,324	264,870	260,515	137,175	142,096	267,101
$I/\sigma(I)$[a]	5.3 (1.9)	26.1 (19.1)	17.3 (4.0)	13.0 (2.6)	10.1 (3.5)	6.6 (1.7)
Redundancy[a]	6.6 (6.2)	6.4 (6.0)	7.1 (6.9)	3.7 (3.5)	3.7 (3.8)	3.5 (3.2)
Overall completeness (%)[a]	98.1 (96.0)	98.1 (97.4)	99.8 (99.8)	98.7 (97.2)	99.2 (98.8)	99.3 (98.7)
Overall R_{merge} (%)[a,b]	9.3 (39.2)	8.8 (42.5)	9.2 (40.4)	9.1 (35.1)	11.2 (38.2)	5.6 (34.7)
Wilson B factor (Å^2)	13.85	13.84	11.87	16.52	16.85	19.81
No. of molecules/asymmetric unit	2	2	2	2	2	2
Refinement statistics						
Resolution limit (Å)	20.4–1.57 (1.59–1.57)	36.5–1.50 (1.52–1.50)	22.3–1.51 (1.53–1.51)	37.1–1.87 (1.89–1.87)	26.2–1.85 (1.87–1.85)	24.7–1.89 (1.90–1.88)
Residues in the core $\phi\psi$ region (%)	96.4	96.7	96.3	96.4	96.2	96.5
No. of atoms/asymmetric unit	11,032	11,413	11,677	11,201	11,118	11,191
No. of solvent atoms	1170	1236	1527	1134	1239	1198
Average temperature factors						
Protein	18.5	17.5	17.5	21.5	24.0	23.2
Ligand/ion	29.1	35.0	33.2	38.9	37.3	48.2
Solvent	29.2	29.2	31.8	34.7	33.3	34.5
Root mean square deviation from ideal values						
Bond lengths (Å)	0.011	0.012	0.011	0.014	0.013	0.009
Bond angles (degrees)	1.049	1.078	1.153	1.112	1.077	1.083
R_{work} (%)[a,c]	21.5 (26.2)	16.2 (22.4)	16.1 (20.3)	15.2 (20.5)	21.2 (28.1)	15.8 (22.6)
R_{free} (%)[a,d]	24.3 (30.5)	17.7 (25.7)	17.8 (21.9)	18.0 (23.7)	26.4 (34.1)	19.0 (27.9)
Ramachandran plot statistics (%)						
Residues in favored regions	96.4	96.7	96.3	96.3	96.1	96.6
Residues in allowed regions	3.6	3.3	3.5	3.7	3.7	3.4
Outliers	0	0	0.2	0	0.2	0

[a] Values in parentheses refer to data for the highest resolution shells.
[b] $R_{merge} = \Sigma_h\Sigma_i|I_{h,I} - \langle I_h\rangle|/\Sigma_h\Sigma i\ I_{h,I}$, where $I_{h,I}$ is the intensity value of the ith measurement of h, and $\langle I_h\rangle$ is the corresponding mean value of I_h for all i measurements.
[c] $R_{work} = \Sigma||F_o| - |F_c||/\Sigma|F_o|$.
[d] R_{free} is an R factor of the refinement evaluated for 5% of reflections that were excluded from the refinement.

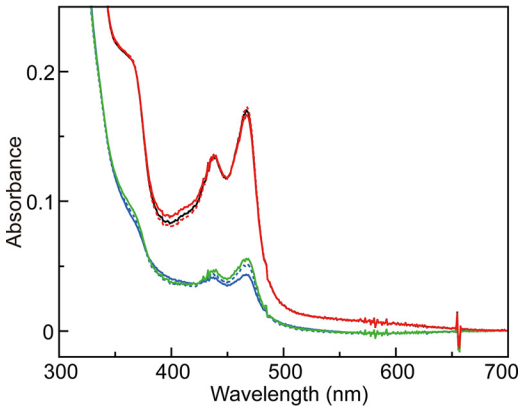

FIGURE 1. **Effects of salts on TPQ_{sq} formation.** UV-visual absorption spectra of TPQ_{sq} generated by anaerobic reaction with 2-PEA (1 mM) as the substrate were measured with 100 μM AGAO monomer in 100 mM HEPES, pH 6.8, in the absence (*black solid line*) and presence of various salts at a final concentration of 10 mM: NaCl (*green solid line*), NH_4Cl (*blue solid line*), KCl (*blue broken line*), Na_2SO_4 (*red broken line*), or NaH_2PO_4 (*red solid line*).

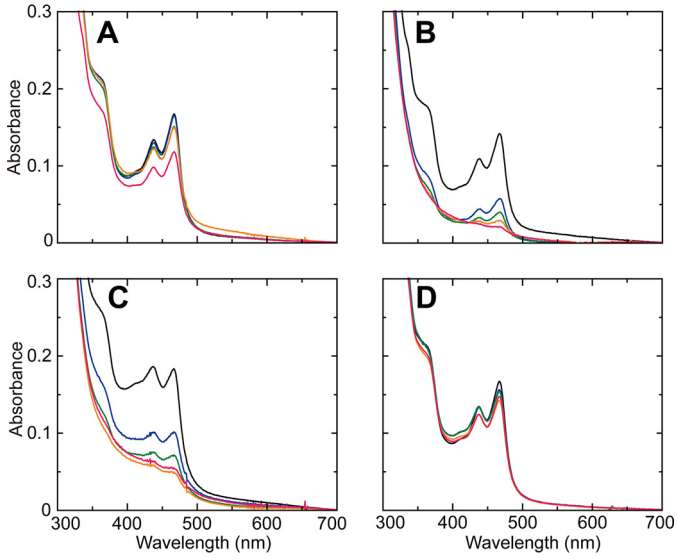

FIGURE 2. **Effects of halide ion concentration on TPQ_{sq} formation.** UV-visual absorption spectra of TPQ_{sq} (generated from 100 μM AGAO monomer and 1 mM 2-PEA) were measured in 100 mM HEPES, pH 6.8, containing 0 (*black*), 5 (*blue*), 10 (*green*), 30 (*orange*), and 50 mM (*red*) NaF (*A*), NaCl (*B*), NaBr (*C*), or NaI (*D*).

TPQ_{amr}, and TPQ_{sq} were similar to those reported previously (29). However, the spectral changes observed in the presence of 100 mM NaCl or 300 mM NaBr could not be fitted to the four-step model. On the basis of the spectral changes and inhibition mechanism described above, it appeared that halide ions (X^-) bound to the TPQ_{amr} state. We therefore proposed a branched model (with the branch connecting TPQ_{ox} to $TPQ_{amr}{\cdot}X^-$; Scheme 1), in which the $TPQ_{amr}{\cdot}X^-$ complex accumulates. The new model provided a reasonable solution to the data fitting of the spectral changes in the presence of NaCl or NaBr. As shown in Table 2, the rate constants of the steps between TPQ_{ox} and TPQ_{sq} ($k_{\pm1}$, $k_{\pm2}$, $k_{\pm3}$, and $k_{\pm4}$) were comparable with those observed without halide ions, although the k_{-3} value was approximately halved. The rate constant of the branching step from TPQ_{amr} to $TPQ_{amr}{\cdot}X^-$ (k_{+5}) (Scheme 1) was estimated to be half that for TPQ_{sq} formation (k_{+4}). The magnitude of these parameters well explains the slow accumulation of $TPQ_{amr}{\cdot}X^-$;

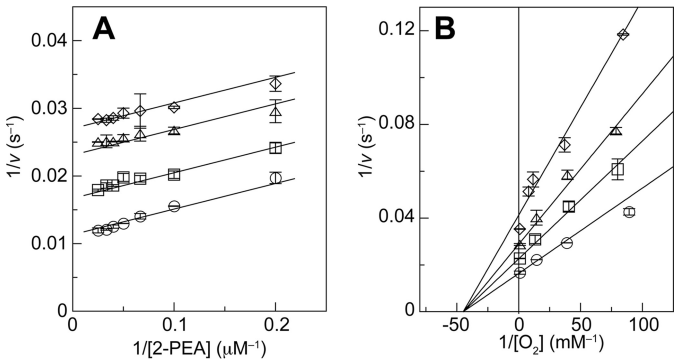

FIGURE 3. **Steady-state kinetics analysis in the presence of NaCl.** *A*, AGAO activity was measured at 30 °C in 50 mM HEPES (pH 6.8) in the presence of 0 (○), 10 (□), 30 (△), or 50 (◇) mM NaCl with systematically varied 2-PEA concentrations. *B*, AGAO activity was measured in solutions containing 40 μM 2-PEA and 0 (○), 12.5 (□), 25 (△), or 50 (◇) mM NaCl with systematically varied solvent O_2 concentrations. Each point represents the mean ± S.E. (*error bars*) from two independent experiments.

TPQ_{sq} is formed initially but gradually converted to $TPQ_{amr}{\cdot}X^-$ via TPQ_{amr}. The deduced absorption spectra of TPQ_{ox}, TPQ_{ssb}, TPQ_{psb}, TPQ_{amr}, and TPQ_{sq} in the presence of NaCl (Fig. 4*G*) and NaBr (Fig. 4*H*) were essentially identical to those observed without halide ions (Fig. 4*E*) and in the presence of 300 mM Na_2SO_4 (Fig. 4*F*). Altogether, these results show that halide ions bind to the TPQ_{amr} form in the reductive half-reaction, thereby inhibiting the formation of TPQ_{sq} from TPQ_{amr}.

Effect of Solvent Viscosity on AGAO Activity—To further probe the equilibrium shift between TPQ_{amr} and TPQ_{sq}, we examined the dependence of catalytic activity on solvent viscosity, which can perturb diffusion-controlled steps, including substrate binding, product release, and conformational changes of the enzyme (58, 59). Glycerol (M_r = 92.1) and sucrose (M_r = 342.3) were used as viscogens. Steady-state kinetic analyses in viscogenic solutions, in which the relative solvent viscosity (η/η^0, where η and η^0 denote viscosities in the presence and absence of the viscogen, respectively) was increased by adding glycerol or sucrose, yielded values of k_{cat}/K_m for 2-PEA that were basically identical to that observed in non-viscogenic solution, whereas the k_{cat} values decreased. The ratio of the viscogen-free k_{cat} value to that in the presence of viscogen (k^0_{cat}/k_{cat}, where k^0_{cat} and k_{cat} denote the rate constants in the absence and presence of the viscogen, respectively) was roughly proportional to the relative solvent viscosity (Fig. 5). This suggests that a diffusion-controlled step(s) is included in the overall reaction consisting of TPQ_{imq}, TPQ_{ssb}, TPQ_{psb}, TPQ_{amr}, TPQ_{sq}, and TPQ_{imq} under steady-state conditions (Scheme 1).

To evaluate the effect of solvent viscosity on each step of the reductive half-reaction, transient kinetic analyses were conducted (Fig. 6). Stopped-flow measurements in the absence and presence of 30% (w/v) glycerol generally produced similar spectral changes, but the formation of TPQ_{sq} was clearly slower in the viscogen's presence (Fig. 6, *A* and *B*, *insets*). Slow TPQ_{sq} formation was evident from the comparison of the traces of absorbance changes at 468 nm specific to TPQ_{sq} (Fig. 6*C*). Further, the rate constants of each step (k_{+1}, k_{+2}, k_{+3}, k_{-1}, k_{-2}, and k_{-3}) in the reductive half-reaction were determined by global

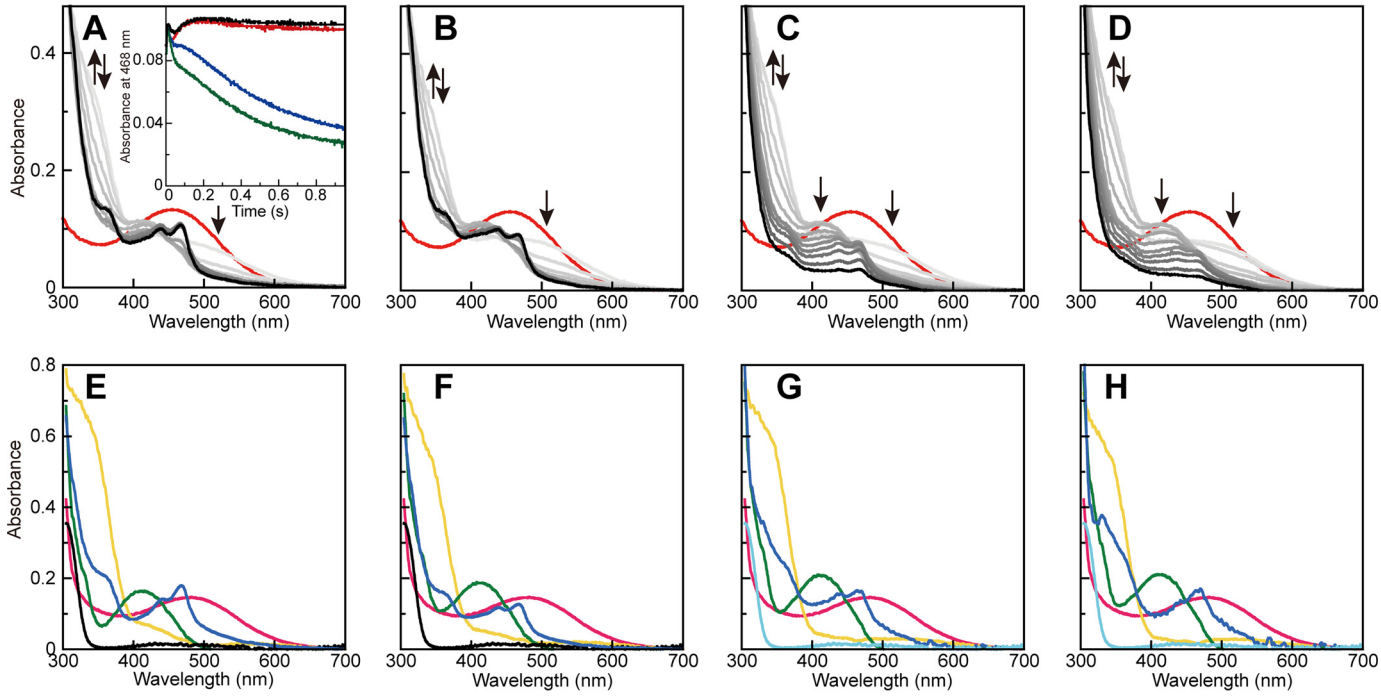

FIGURE 4. **Spectral changes during the reductive half-reaction with 2-PEA.** UV-visible absorption spectra were recorded after mixing AGAO (100 μM monomer) with 2 mM 2-PEA (*A*), 2 mM 2-PEA plus 300 mM Na_2SO_4 (*B*), 2 mM 2-PEA plus 100 mM NaCl (*C*), or 2 mM 2-PEA plus 300 mM NaBr (*D*) in 50 mM HEPES buffer, pH 6.8, at 4 °C under anaerobic conditions. The spectra obtained at 0 (*red*), 2.30, 3.84, 6.4, 8.96, 14.1, 24.3, 44.8, 117, 209, 332, 600, and 1023 ms are shown using *darker colors* to represent later times. The *arrows* indicate the direction of the spectral changes. Deduced absorption spectra are shown for TPQ_{ox} (*red*), TPQ_{ssb} (*yellow*), TPQ_{psb} (*green*), TPQ_{amr} (*black*), and TPQ_{sq} (*blue*) in *E*, *F*, *G*, and *H*, calculated from the measurements of *A* (no salt), *B* (300 mM Na_2SO_4), *C* (100 mM NaCl), and *D* (300 mM NaBr), respectively. The absorption spectra for $TPQ_{amr}{\cdot}X^-$ (*cyan*) generated during the experiments using 100 mM NaCl (*C*), and 300 mM NaBr (*D*) are shown in *G* and *H*, although they are defined to be identical to that of TPQ_{amr} (*black*). The *inset* of *A* shows the time course of the absorbance at 468 nm in the spectral changes of *A* (no salt, *red*), *B* (300 mM Na_2SO_4, *black*), *C* (100 mM NaCl, *blue*), and *D* (300 mM NaBr, *green*).

TABLE 2

Kinetic constants for each step of the reductive half-reaction in the absence and presence of various salts and a viscogen at 4 °C

	No addition	+300 mM Na_2SO_4	+100 mM NaCl	+300 mM NaBr	+30% (w/v) glycerol
k_{+1} (s^{-1})[a]	887 ± 0.2	880 ± 0.3	887 ± 0.6	880 ± 0.08	871 ± 0.03
k_{-1} (s^{-1})	531 ± 0.8	529 ± 0.05	530 ± 0.2	528 ± 2	560 ± 0.02
k_{+2} (s^{-1})	206 ± 0.04	207 ± 0.1	206 ± 0.1	207 ± 0.3	201 ± 0.006
k_{-2} (s^{-1})	34 ± 0.008	34 ± 0.02	34 ± 0.02	34 ± 0.07	34 ± 0.001
k_{+3} (s^{-1})	102 ± 0.06	102 ± 0.05	102 ± 0.06	103 ± 0.2	100 ± 0.003
k_{-3} (s^{-1})	127 ± 8	127 ± 5	63 ± 3	76 ± 7	134 ± 0.007
k_{+4} (s^{-1})	39 ± 9	39 ± 6	32 ± 6	23 ± 11	15 ± 0.001
k_{-4} (s^{-1})	17 ± 3	12 ± 2	15 ± 4	21 ± 6	6 ± 0.001
k_{+5} (s^{-1})[a]			15 ± 7	21 ± 12	
k_{-5} (s^{-1})			5 ± 2	9 ± 3	

[a] Determined as a first-order rate constant at constant and excess concentrations of amine substrate (2-PEA) and halide ions.

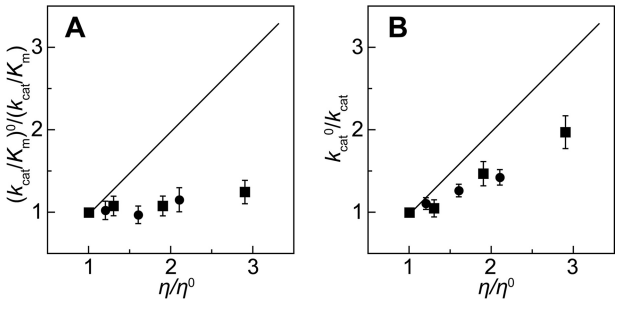

FIGURE 5. **Dependence of steady-state kinetic parameters on solvent viscosity.** The ratios of k_{cat}/K_m (*A*) and k_{cat} (*B*) in the presence and absence of viscogen at 4 °C were plotted against the relative solvent viscosity, η/η^0, where zero denotes the value in the absence of viscogen. *Black circles* and *squares*, data points for glycerol and sucrose, respectively. A *thin black line* denotes the theoretical result for a completely diffusion-controlled process with a slope of 1.0. *Error bars*, S.D. ($n = 2$).

analysis according to the four-step model starting from TPQ_{ox} and ending at TPQ_{sq} (Scheme 1). Of these rate constants, k_{+1}, k_{+2}, k_{+3}, k_{-1}, k_{-2}, and k_{-3} were independent of the glycerol concentration, but the values of k_{+4} and k_{-4} (which relate to the interconversion of TPQ_{amr} and TPQ_{sq}) decreased in proportion to the glycerol concentration (Table 2), showing that this step is diffusion-controlled. For detailed analysis, the ratios of k^0/k were plotted against the relative solvent viscosity, η/η^0 (Fig. 6*D*), where k^0 and k are the rate constants (k_{+2}, k_{-2}, k_{+4}, and k_{-4}) in the absence and presence of viscogen (glycerol), respectively. The ratios of k^0_{+4}/k_{+4} and k^0_{-4}/k_{-4} increased significantly in proportion to the relative solvent viscosity, although the slope of the fitted line (0.50) indicated a partial effect; an entirely diffusion-controlled reaction would give a slope of 1.0 (60) (Fig. 6*D*). The ratios of the other rate constants were almost independent of the relative solvent viscosity (*e.g.*

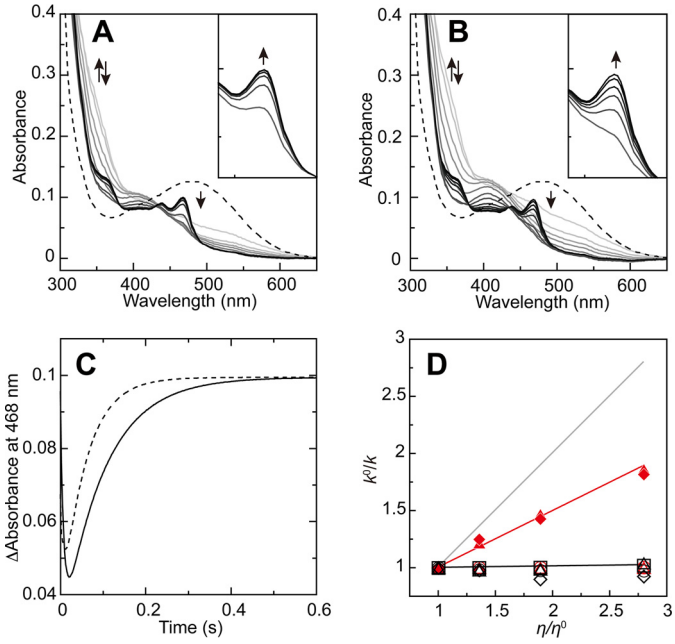

FIGURE 6. **Effects of viscosity on the reductive half-reaction.** UV-visible absorption spectra were recorded in 50 mM HEPES buffer, pH 6.8, at 4 °C under anaerobic conditions upon mixing AGAO (100 μM monomer) with 2 mM 2-PEA (*A*) or 2 mM 2-PEA (*B*) in the presence of 30% (w/v) glycerol. The spectra obtained at 0 (*broken line*), 2.30, 3.84, 6.4, 8.96, 14.1, 24.3, 44.8, 117, 209, 332, 600, and 1023 ms are shown with *darker colors* representing later times. The *arrows* indicate the direction of the spectral changes. The *insets* expand the 440–500 nm region for easier inspection of the spectral changes. *C*, absorbance at 468 nm was monitored during the spectral change of 2 mM 2-PEA (*broken line*) (*A*) or 2 mM 2-PEA (*B*) in the presence of 30% (w/v) glycerol (*solid line*) at 0–0.6 s. *D*, ratios of the rate constants (k^0_{+2}/k_{+2} (*red open circle*), k^0_{-2}/k_{-2} (*red open triangle*), k^0_{+4}/k_{+4} (*red triangle*), and k^0_{-4}/k_{-4} (*red rhombus*) determined in solutions of up to 30% (w/v) glycerol and k^0_{+2}/k_{+2} (*black open circle*), k^0_{-2}/k_{-2} (*black open square*), k^0_{+4}/k_{+4} (*black open triangle*), and k^0_{-4}/k_{-4} (*black open rhombus*) determined in solutions of up to 30% (w/v) sucrose) were plotted against the relative viscosity. S.D. values were less than 0.03% at all points ($n = 2–4$) and therefore are not shown with error bars. *Thick lines* (*black* and *red*) denote fitted linear lines for the k^0_{+4}/k_{+4} values for sucrose and glycerol, respectively. The *gray solid line* denotes the theoretical result for a completely diffusion-controlled process with a slope of 1.0.

slope = 0.003 for k^0_{+2}/k_{+2}) (Fig. 6*D*). The reaction step connecting TPQ_{amr} and TPQ_{sq} involves neither substrate binding nor product release. Thus, these findings show that the interconversion of TPQ_{amr} and TPQ_{sq} is accompanied by a conformational change(s) of the enzyme. Reducing the viscogen's access to the region undergoing the conformational change could reduce its effective concentration, explaining the partial effect indicated by the k^0/k slope of ~0.5. It is therefore likely that the conformational change(s) occurs somewhere in the protein interior, such as the buried active site (most likely in the TPQ cofactor itself). Supporting this, we were unable to observe any effect of solvent viscosity on the rate constants k_{+4} and k_{-4} when using 30% (w/v) sucrose as the viscogen; sucrose's molecular size is 3.7-fold greater than that of glycerol, so it probably cannot penetrate into the active site cavity (Fig. 6*D*).

Reductive Half-reaction in Crystals—To obtain structural insights into the interconversion between TPQ_{amr} and TPQ_{sq}, the AGAO crystals were reacted anaerobically with substrates in the presence or absence of halide ions under six different conditions (Table 3), and the intermediates formed were freeze-trapped for structural determination. Before x-ray analysis, these crystals were subjected to single-crystal microspec-

TABLE 3
Summary of crystal soaking conditions and active-site features determined by x-ray crystallographic analysis

	$AGAO_{PEA}$	$AGAO_{HTA}$	$AGAO_{ETA/HCl}$[a]	$AGAO_{PEA/NaCl}$	$AGAO_{PEA/NaBr}$	$AGAO_{NaBr}$
Soaking conditions	2-PEA, anaerobic	Histamine, anaerobic	Ethylamine, anaerobic	2-PEA, NaCl, anaerobic	2-PEA, NaBr, anaerobic	NaBr, aerobic
Assigned TPQ species	TPQ_{sq}	TPQ_{sq}	TPQ_{amr}	TPQ_{psb}	TPQ_{psb}	TPQ_{ox}
Conformation of TPQ	On copper	On copper	Off copper	Off copper	Off copper	Off copper
Copper coordination geometry	Tetrahedral	Tetrahedral	Square pyramidal	Square pyramidal	Square pyramidal	Square pyramidal
Presumed copper valence	Cu(I)	Cu(I)	Cu(II)	Cu(II)	Cu(II)	Cu(II)
Axial ligand of copper atom (distance, Å)	TPQ_{sq} C4-OH (2.8)	TPQ_{sq} C4-OH (2.7)	Cl^- (2.5)	Cl^- (2.3)	Br^- (2.5)	Water (2.6)

[a] Data for chain A.

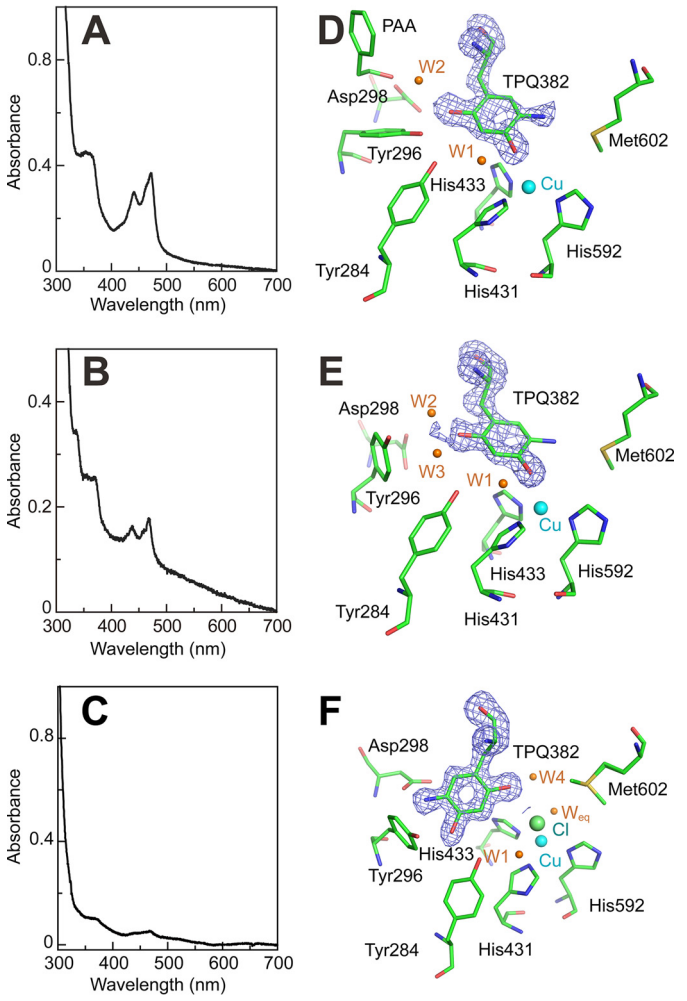

FIGURE 7. **Catalytic intermediate structures and UV-visible absorption spectra of AGAO after reaction with 2-PEA, histamine, and ethylamine hydrochloride.** AGAO crystals were anaerobically soaked with excess 2-PEA, histamine, or ethylamine hydrochloride, and the x-ray structures of the resulting crystals were determined. UV-visible absorption spectra for single crystals of $AGAO_{PEA}$ (*A*), $AGAO_{HTA}$ (*B*), and $AGAO_{ETA/HCl}$ (*C*) were measured before x-ray exposure. The active-site structures of $AGAO_{PEA}$ (*D*), $AGAO_{HTA}$ (*E*), and $AGAO_{ETA/HCl}$ (*F*) are shown *superimposed* on the $F_o - F_c$ omit map (*blue mesh*) for residue 382 contoured at 3.5 σ. Active-site residues are represented by *green stick models*. Water molecules and copper centers are represented by *brown* and *cyan spheres*, respectively. All molecular drawings were generated using PyMOL.

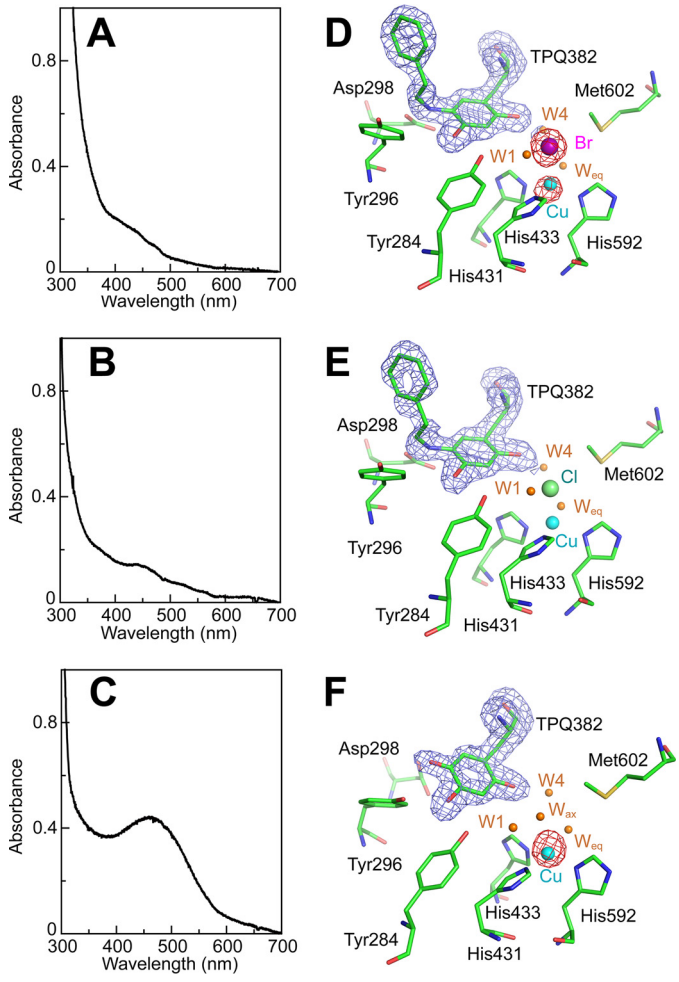

FIGURE 8. **Active-site structures and UV-visible absorption spectra of AGAO soaked with halide salts and/or substrates.** AGAO crystals were anaerobically soaked with excess 2-PEA in the presence of NaBr (*A* and *D*) or NaCl (*B* and *E*). *C* and *F* show results for AGAO crystals soaked only with NaBr under aerobic conditions. UV-visible absorption spectra for the single crystals of $AGAO_{PEA/NaBr}$ (*A*), $AGAO_{PEA/NaCl}$ (*B*), and $AGAO_{NaBr}$ (*C*) were measured before x-ray exposure. The refined model of the active site structures of $AGAO_{PEA/NaBr}$ (*D*), $AGAO_{PEA/NaCl}$ (*E*), and $AGAO_{NaBr}$ (*F*) are shown *superimposed* on the $F_o - F_c$ omit map (*blue mesh*) for residue 382 contoured at 3.5 σ. Bromine-anomalous maps contoured at 8 σ are represented by *red meshes* in the active sites of $AGAO_{PEA/NaBr}$ (*D*) and $AGAO_{NaBr}$ (*F*). The anomalous dispersion of the copper atom is pronounced although the wavelength of the used x-ray (0.919 Å) deviated from the peak wavelength of the copper atom (1.3808 Å), and an anomalous peak (about 18 σ) was detected on the copper site of the active center as well as for the bromine atom. Active-site residues are represented by *green stick models*. Water molecules and copper atoms are represented by *brown* and *cyan spheres*, respectively. All molecular drawings were generated using PyMOL.

trophotometry to identify the reaction intermediates present within them (29, 40, 41). The absorption spectra of the frozen crystals anaerobically soaked with 4 mM 2-PEA or 10 mM histamine (these crystals were designated $AGAO_{PEA}$ and $AGAO_{HTA}$, respectively) (Fig. 7, *A* and *B*) were very similar to that of TPQ_{sq} for the enzyme in solution, showing specific absorption peaks around 365, 438, and 465 nm (Fig. 1). In contrast, the crystals anaerobically soaked with 50 mM ethylamine (hydrochloride) ($AGAO_{ETA/HCl}$) gave a rather peakless spectrum resembling that of TPQ_{amr} (Fig. 7*C*), although small TPQ_{sq}-like peaks remained. Furthermore, in the presence of 100 mM NaCl or 300 mM NaBr, the crystals prepared by anaerobic soaking with 4 mM 2-PEA (designated $AGAO_{PEA/NaCl}$ and $AGAO_{PEA/NaBr}$, respectively) exhibited absorption spectra (Fig. 8, *A* and *B*) that were distinct from those of TPQ_{sq} and TPQ_{amr} but comparable with that of TPQ_{psb} for the enzyme in solution (Fig. 4*E*). To identify the halide ion-binding site(s) in the unreacted enzyme, the crystal was aerobically soaked with 300 mM NaBr alone ($AGAO_{NaBr}$). This yielded a spectrum identical to that of TPQ_{ox} because the reaction could not proceed (Fig. 8*C*). These crystal absorption spectra revealed that the reductive half-reaction occurred in all of the crystals except for $AGAO_{NaBr}$ and that the accumulation of the TPQ_{psb}, TPQ_{amr}, or TPQ_{sq} intermediates could be induced by soaking the crystals with appropriate amine substrates in the presence or absence of halides (Table 3).

The overall structures determined for $AGAO_{PEA}$, $AGAO_{HTA}$, $AGAO_{ETA/HCl}$, $AGAO_{PEA/NaCl}$, $AGAO_{PEA/NaBr}$, and $AGAO_{NaBr}$ were comparable with that of resting AGAO (Protein Data

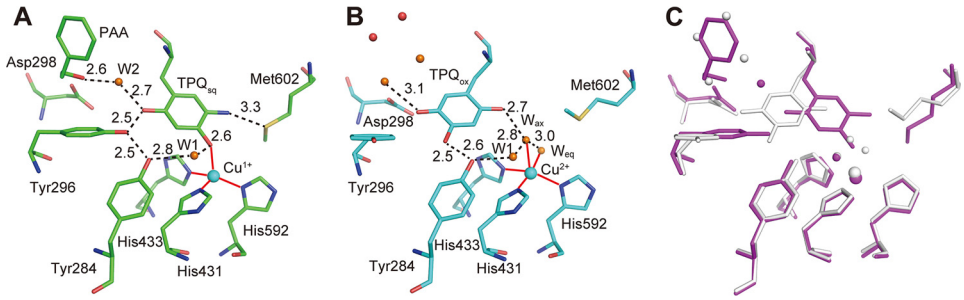

FIGURE 9. **Interactions in the on-copper and off-copper conformations.** The active sites of $AGAO_{PEA}$ (*A*) and the substrate-free and oxidative form of AGAO (Protein Data Bank code 1IU7) (*B*), in which the TPQ ring has on-copper and off-copper conformations, respectively, are drawn showing hydrogen bonds (*dotted lines*) and ligation to the copper centers (*red lines*). Estimated hydrogen bond lengths are shown in Å. The superposition of *A* and *B* is shown in *C*, in which the on-copper (*A*) and off-copper (*B*) structures are *colored* in *purple* and *gray*, respectively. All molecular drawings were generated using PyMOL.

Bank code 1IU7), with root mean square deviations for the main-chain atoms within ~0.4–0.5 Å. In these crystal structures, we assigned the chemical structures of TPQ based on its absorption spectra (Table 3) and constructed the active-site structures using the assigned models of TPQ in different conformations, which were built to coincide with the $F_o - F_c$ omit maps (Figs. 7 and 8). The two monomers (chains A and B) of the homodimer in the asymmetric unit of the crystals showed essentially identical active-site structures except for those in the $AGAO_{ETA/HCl}$ crystal, in which active-site residues, including TPQ and water molecules, had slightly different conformations and electron densities between the two monomers.

The most notable finding from the crystal structures was that the TPQ_{sq} moieties in $AGAO_{PEA}$ and $AGAO_{HTA}$ had an on-copper conformation with ~100% occupancy, with the 4-OH group of TPQ_{sq} projecting toward the copper center at a distance of 2.7–2.9 Å (Fig. 7, *D* and *E*) and the 5-NH_2 group positioned opposite to the catalytic base (Asp-298) in close proximity to Met-602. This is the first x-ray structure of CAO with TPQ_{sq} being exclusively copper-ligating, although an on-copper TPQ_{sq} structure with ~65–70% occupancy was recently reported for HPAO-1 crystals reduced with methylamine in a low oxygen environment at pH 8.5 (39). The copper center in $AGAO_{PEA}$ and $AGAO_{HTA}$ was tetrahedrally coordinated with the 4-OH group of TPQ at the "axial" position and the imidazole groups of three histidines (His-431, His-433, and His-592) at the "equatorial" positions. No water molecules were coordinated to the copper center. On the other hand, TPQ_{amr} in $AGAO_{ETA/HCl}$ had an off-copper conformation with ~100% occupancy, in which the 5-NH_2 group of TPQ_{amr} was positioned close to Asp-298 and the 4-OH group was hydrogen-bonded to the Tyr-284 side chain rather than coordinating to the copper center (Fig. 7*F*). The off-copper conformation was the sole conformer in chain A. However, both the off-copper and on-copper conformers were present (at a relative abundance of about 6:4) in chain B. Probably, the minor on-copper conformation in chain B was partly responsible for the crystals' small TPQ_{sq}-like absorption peaks (Fig. 7*C*). The spectrophotometrically assigned TPQ_{psb} moiety of $AGAO_{PEA/NaCl}$ and $AGAO_{PEA/NaBr}$ also had an off-copper conformation, in which the C5 position of TPQ was connected to additional electron density corresponding to the phenylethyl moiety of the product phenylacetaldehyde (PAA) via a covalent linkage in the form of an imine bond (Fig. 8, *D* and *E*).

The binding of several halide ions was detected in the $AGAO_{ETA/HCl}$, $AGAO_{PEA/NaCl}$, $AGAO_{PEA/NaBr}$, and $AGAO_{NaBr}$ crystals (2 and 5 Cl^- ions/dimer in $AGAO_{ETA/HCl}$ and $AGAO_{PEA/NaCl}$, respectively, and 8 Br^- ions/dimer in $AGAO_{PEA/NaBr}$ and $AGAO_{NaBr}$), as judged by the anomalous peaks (over 7 σ) generated by the Br^- ion and the electron densities (over 8 σ) of the Cl^- ion, which were clearly greater than those of water molecules (less than 5 σ). The Cl^- ions identified in $AGAO_{ETA/HCl}$ derived from the substrate (ethylamine hydrochloride), which was present at a high concentration (50 mM). In the halide-bound complexes, a Br^- or Cl^- ion was found to occupy the axial coordination site of the active-site copper center in the $AGAO_{ETA/HCl}$, $AGAO_{PEA/NaCl}$, and $AGAO_{PEA/NaBr}$ structures (Figs. 7*F* and 8 (*D* and *E*) and Table 3). These are the first x-ray crystal structures of CAO with an anionic inhibitor (57, 61, 62) bound to the active site copper center. In contrast, the axial position in $AGAO_{NaBr}$ was occupied by a water molecule rather than Br^- (Fig. 8*F* and Table 3); Br^- ions instead bound to the protein surface in a seemingly nonspecific fashion. Similar behavior was observed in $AGAO_{PEA/NaBr}$. Specific binding of a halide ion at the axial position of the active-site copper center only occurred in crystals that had been anaerobically soaked with substrate, strongly suggesting that the uncompetitive inhibition of the steady-state reaction by halide ions with respect to 2-PEA is due to their ability to bind to the copper center in the reaction intermediates, in which TPQ is reduced with substrates, rather than to the copper center in the free enzyme. It also suggests that the axial ligand-binding position of the copper center exhibits a stronger preference for halide ions in the substrate-reduced form of AGAO than in the resting form.

Comparison of the on-copper TPQ_{sq} structures of $AGAO_{PEA}$ and $AGAO_{HTA}$ with the off-copper TPQ_{ox} structure in resting AGAO (Protein Data Bank code 1IU7) revealed that most active-site residues (except for Tyr-296 and Met-602), water molecules, and the copper center are retained in almost the same positions and conformations (Fig. 9). In the TPQ_{sq} structures, the side-chain phenol ring of Tyr-296 rotates ~80° around the Cα–Cβ bond to participate in a hydrogen-bonding network involving two water molecules (W1 and W2); the 2-OH, 4-OH, and 5-NH_2 groups of TPQ_{sq}; the 4-OH group of Tyr-284; and the Sδ atom of Met-602 (Fig. 9*A*). The on-copper conformation is probably stabilized by this hydrogen-bonding

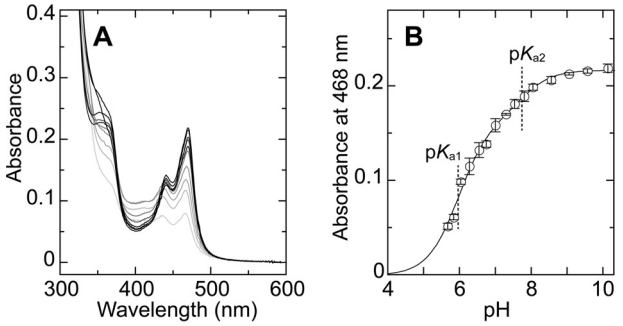

FIGURE 10. **pH dependence of TPQ_{sq} formation.** *A*, 100 μM AGAO monomer was anaerobically reduced with 1 mM 2-PEA at various pH values in the presence of 100 mM Na_2SO_4, and UV-visual absorption spectra of AGAO were measured at 25 °C after a 5-min preincubation. *B*, absorbance at 468 nm specific to TPQ_{sq} was plotted against pH. A *solid line* indicates the theoretical line obtained by data fitting. The spectra at pH 5.67, 6.02, 6.53, 6.99, 7.52, 8.03, 8.54, 9.04, 9.55, and 10.12 are shown with *darker colors* corresponding to higher pH values. Each point represents the mean ± S.E. (*error bars*) from 2–4 independent experiments.

network, allowing the direct coordination of the 4-OH group of TPQ to the copper center, which would facilitate rapid, ligand-to-metal charge transfer-like electron transfer from TPQ_{amr} to Cu(II) to form the TPQ_{sq}·Cu(I) state.

In keeping with the single-crystal microspectrophotometric observations, a TPQ_{psb}-like intermediate was identified in the $AGAO_{PEA/NaBr}$ and $AGAO_{PEA/NaCl}$ structures, which was probably formed by a condensation reaction between the amino group of TPQ_{amr} (in the off-copper form) and the aldehyde group of the reaction product PAA, which remains in the substrate-binding hydrophobic pocket (Fig. 8, *D* and *E*); PAA was indeed found to remain bound in the $AGAO_{PEA}$ structure (Fig. 7*D*), as reported previously for the 2-PEA-reduced *E. coli* CAO crystals (63). This assumption is also supported by the finding that the TPQ_{psb} observed in $AGAO_{PEA/NaBr}$ and $AGAO_{PEA/NaCl}$ had a *cis*-configuration, whereas the TPQ_{psb} formed during the reductive half-reaction of the D298A mutant of AGAO had a *trans*-configuration (29). The absence of the product aldehydes (imidazole-4-acetaldehyde and acetaldehyde) in the $AGAO_{HTA}$ and $AGAO_{ETA/HCl}$ structures is probably due to their low affinities for the substrate-binding pocket of AGAO; for comparative purposes, the K_m values for histamine (1.2 mM) and ethylamine (170 mM) are 220- and 30,000-fold higher, respectively, than that for 2-PEA (5.4 μM) (41). Overall, these findings indicate that in the $AGAO_{PEA/NaBr}$ and $AGAO_{PEA/NaCl}$ crystals, the binding of halide ions (Br^- and Cl^-) to the axial position of the copper center prevented TPQ_{amr} from adopting the on-copper conformation, causing it to back-react with PAA to form a TPQ_{psb} configuration distinct from that formed during the reductive half-reaction.

Effect of pH on the Equilibrium between TPQ_{amr} and TPQ_{sq}—The equilibrium between TPQ_{amr} and TPQ_{sq} in AGAO has been reported to shift toward TPQ_{sq} under alkaline conditions (35), which suggests that an ionizable group(s) plays a role in triggering the conformational change of the cofactor. We therefore used spectrophotometry to investigate the effect of pH on the equilibrium between TPQ_{amr} and TPQ_{sq}. The reductive half-reaction was performed with 2-PEA as the substrate at pH values ranging from 5.7 to 10.1 with a constant ionic strength (Fig. 10*A*); AGAO is stable in this pH range. The TPQ_{sq}-specific absorption peaks at about 440 and 470 nm, and the shoulder at about 350 nm increased in intensity as the pH rose from 5.7 to 8.5 but did not change further above pH 8.5, indicating that the equilibrium shifted toward TPQ_{sq} above pH 8.5. By plotting the absorbance at 468 nm, to which TPQ_{amr} makes no contribution, against the pH (Fig. 10*B*) and fitting the data to Equation 1, two ionizable groups with apparent pK_a values of 5.96 ± 0.05 (pK_{a1}) and 7.74 ± 0.19 (pK_{a2}) were found to be involved in the equilibrium shift from TPQ_{amr} to TPQ_{sq}. Judging from the magnitude of pH-independent absorbance values ($C_1 = 0.164$, $C_2 = 0.053$), deprotonation of the ionizable group with pK_a = 5.96 contributes predominantly to the equilibrium shift.

Discussion

The results presented above demonstrate that the off-copper and on-copper conformations of TPQ are readily interconvertible during the reductive half-reaction with various amine substrates and in the presence of halide ions. In the steps prior to the formation of TPQ_{amr} (Scheme 1), the catalytic reaction proceeds with TPQ always maintained in the off-copper conformation irrespective of its chemical state (29, 40, 41). In the TPQ_{ssb} and TPQ_{psb} states, the distal part of the substrate amine is anchored to the substrate-binding pocket, preventing the TPQ ring from adopting the on-copper conformation (29). However, once TPQ_{psb} is hydrolyzed, the reduced TPQ gains the conformational flexibility that enables facile interconversion between the off-copper and on-copper conformations.

In the on-copper conformation of TPQ_{sq} as observed in the $AGAO_{PEA}$ and $AGAO_{HTA}$ structures (Fig. 9, *A* and *B*), the active-site copper center is equatorially coordinated by three imidazole groups from His residues without the equatorial water ligand seen in the resting TPQ_{ox}·Cu(II) state (17) and other intermediates formed in the reductive half-reaction (Figs. 7 and 8). A similar decrease in the number of equatorial ligands at the copper center was observed in extended x-ray absorption fine structure studies on various dithionite-treated CAOs, in which Cu(II) is reduced to Cu(I) (64). It is therefore suggested that the tetrahedrally coordinated copper centers observed in the $AGAO_{PEA}$ and $AGAO_{HTA}$ crystals are probably in the Cu(I) oxidation state, as was proposed in a recent paper on the structure of methylamine-reduced HPAO-1 (39). Based on the full occupancy of the modeled TPQ_{sq} in the electron density map, essentially all of their TPQ is assumed to be in the TPQ_{sq} state. Taken together, these results show that the on-copper conformation is a consequence of $1e^-$ transfer from TPQ_{amr} to Cu(II) to form the TPQ_{sq}·Cu(I) state. In contrast, a water molecule (W_{eq}) was identified as an equatorial ligand of the copper atom in the $AGAO_{ETA/HCl}$ crystal, with observed electron densities of 3.7 and 2.3 σ in crystallographically distinguishable chains A and B, respectively. In addition, a Cl^- ion was found to occupy an axial position in the copper complex (Fig. 7*C*), whose five-coordinate square pyramidal structure suggests that the copper is in the Cu(II) oxidation state, especially in chain A, for which TPQ is mostly in the off-copper TPQ_{amr} state based on its absorption spectrum and x-ray structure. We have so far observed neither the off-copper TPQ_{sq}·Cu(I) form nor the on-copper TPQ_{amr}·Cu(II) form, strongly suggesting that the $1e^-$ transfer occurs exclusively in the on-copper conformation of

TPQ_{amr}. This also leads to the suggestion that before the formation of the TPQ_{sq}·Cu(I) state, the TPQ quinone ring moves from the off-copper to the on-copper conformation.

The spectroscopic data from the transient kinetics experiments showed that the formation of TPQ_{sq} is dependent on solvent viscosity (Fig. 6*D*), further supporting the occurrence of a conformational change in TPQ during the last step of the reductive half-reaction. Because the rate constants of this step (k_{+4}) were determined from the absorbance changes associated with TPQ_{sq}, they represent the rates of both the conformational change of TPQ and the subsequent electron transfer from TPQ_{amr} to Cu(II). The same presumption holds for the rate constants of the electron transfer (k_{ET}) determined previously by temperature-jump relaxation studies (33, 35, 65), which varied from 60–75 s^{-1} (*Arthrobacter* P1 methylamine oxidase) (65) to 20,000 s^{-1} (*P. savitum* CAO) (33). The latter extremely large rate constant was attributed to the intrinsic k_{ET} and interpreted to mean that the TPQ cofactor is in close proximity (~3 Å) to the copper center (33) (*cf.* the distance of 2.6 Å between the TPQ 4-O atom and the copper center; Fig. 9). It is thus likely that the smaller rate constants determined previously (k_{ET}) and in this study (k_{+4}) mainly reflect the rate constants for the conformational change of the TPQ cofactor, in agreement with the suggestion that conformationally "gated" or controlled electron transfer is plausible (33). An extended x-ray absorption fine structure study (64) also raised the possibility that variations in the redox potentials or the effective electron transfer distance between TPQ_{amr} and Cu(II) may control k_{ET}. The difference between the rate constants for AGAO determined here (Table 2; k_{+4} = 39 s^{-1} at 4 °C, pH 6.8) and previously (k_{ET} = 73 s^{-1} at 5 °C, pH 7.2) (37) is probably due to subtle differences in temperature and pH, both of which strongly affect the equilibrium between TPQ_{amr}·Cu(II) and TPQ_{sq}·Cu(I) (33, 35, 37, 39, 65) (Fig. 10); at higher pH values and temperatures, the equilibrium shifts toward TPQ_{sq}·Cu(I), which suggests a ΔH value of >0 for the conformational change of TPQ. Finally, it should be noted that the rate constants of the conformational change are appreciably larger than the k_{cat} value (17 s^{-1}) determined by steady-state kinetics under the same conditions (at 4 °C and pH 6.8), supporting the hypothesis that the conformational change of the cofactor can occur within the overall turnover reaction.

Based on the pH dependence of the equilibrium between TPQ_{amr} and TPQ_{sq}, it is suggested that deprotonation of two ionizable groups with pK_a values of 5.96 ± 0.05 and 7.74 ± 0.19 (Fig. 10*B*) facilitates the equilibrium shift toward TPQ_{sq}. Among several ionizable groups in the active site (5-NH_2 (estimated pK_a, 5.88), 4-OH (9.59), and 2-OH (11.62) groups of TPQ_{amr} (54); the carboxyl group of Asp-298 (7.5 ± 0.20) (29); and the water axially coordinated to the copper atom (~7.5) (66)), the 5-NH_2 group of TPQ_{amr} is most likely assigned to the group with the lower pK_a value (5.96) and mainly contributes to the equilibrium shift toward TPQ_{sq}, with the neutral form of TPQ_{amr} that is the major form at pH >7 being the direct precursor to TPQ_{sq} (Scheme 1). Furthermore, the neutral form of TPQ_{amr} is only weakly tethered in the active site, forming neither electrostatic interactions nor charge-assisted hydrogen bonds (67) with surrounding residues. It should thus be amenable to facile conformational change. The ionizable group with the higher pK_a value (7.74), although contributing insignificantly to the equilibrium shift toward TPQ_{sq}, may be ascribed to the 4-OH group of TPQ_{sq} with a pK_a value of 6.39 determined with a model compound (68), rather than the same group in TPQ_{amr} (pK_a 9.59) (54); deprotonation of the 4-OH group of TPQ_{sq} is expected to stabilize the TPQ_{sq} form (see Scheme 1). If this is the case, deprotonation of the 4-OH group would occur after the conformational change of the TPQ ring and the electron transfer from TPQ_{amr} to Cu(II). A notable increase of the pK_a value (from 6.39 to 7.74) may be conceivable to occur in the hydrophobic active site of CAOs, as observed for the carboxyl group of the catalytic base Asp-298 with a significantly high pK_a value (7.5 ± 0.20) (29).

The TPQ_{amr} structures have been determined previously with the substrate-reduced forms of *E. coli* CAO and HPAO-1 (Protein Data Bank codes 1D6U and 4EV2, respectively), in which the axial positions of the copper atom are occupied by water and a dioxygen species, respectively. Comparison of these structures with the TPQ_{amr} of AGAO bound with a chloride ion ($AGAO_{ETA/HCl}$) has revealed that the TPQ_{amr} ring is tilted anticlockwise by about 20° (rigid body rotation around the Cβ–Cγ bond) in AGAO (Fig. 11*A*). This ~20° tilting of the TPQ ring appears to result from the minuscule movement (by 0.4 Å) of the position of the 2-OH group of TPQ_{amr}, probably due to the repulsion from the axially coordinated chloride ion that has a larger van der Waals radius than water and a dioxygen species. Consequently, the 5-NH_2 group approaches within hydrogen bond distance (2.8 Å) to the carboxyl group of Asp-298 (Fig. 11*A*), which is predominantly protonated at crystallization pH of 6.8, thereby lowering the nucleophilicity of the 5-NH_2 group. The hydrogen bond may also stabilize the tilted conformation of TPQ_{amr} even after the halide ion is released (in the step of k_{-5} in Scheme 1). In addition, the aldehyde group of the product PAA that remains bound in $AGAO_{PEA}$ is located rather distant (3.2 Å) from the 5-NH_2 group of TPQ_{amr} in the $AGAO_{ETA/HCl}$ structure to undergo the nucleophilic attack (Fig. 11*B*). These structural consequences well explain the significantly decreased rate constant (k_{-3}) for the back-formation of TPQ_{psb} in the presence of halide ions (Table 2). Moreover, the geometry of the 5-NH_2 group of TPQ_{amr} relative to the aldehyde carbon atom of PAA strongly suggests that the nucleophilic attack occurs from the *si* face of the carbonyl carbon, leading to the formation of TPQ_{psb} in *cis*-configuration (*cis*-TPQ_{psb}) (Fig. 11*D*), unlike the formation of TPQ_{psb} in *trans*-configuration (*trans*-TPQ_{psb}) from TPQ_{ssb} in the forward reductive half-reaction of the D298A mutant (Fig. 11*C*) (29).

Monovalent anions, such as cyanide and azide, were reported to be inhibitors of various CAOs, showing competitive, noncompetitive, uncompetitive, or mixed type inhibition with respect to the amine substrate and dioxygen (57, 61, 62). For AGAO, cyanide is an uncompetitive inhibitor with respect to the amine substrate, and azide is a noncompetitive inhibitor with respect to both amine and dioxygen (57, 61). Although the inhibition patterns of halide ions (uncompetitive and noncompetitive with respect to amine substrate and dioxygen, respectively) (Fig. 3) for AGAO are similar to those of azide and cyanide, their effects on the equilibrium between TPQ_{amr} and TPQ_{sq} are very different. Halide ions inhibit TPQ_{sq} formation

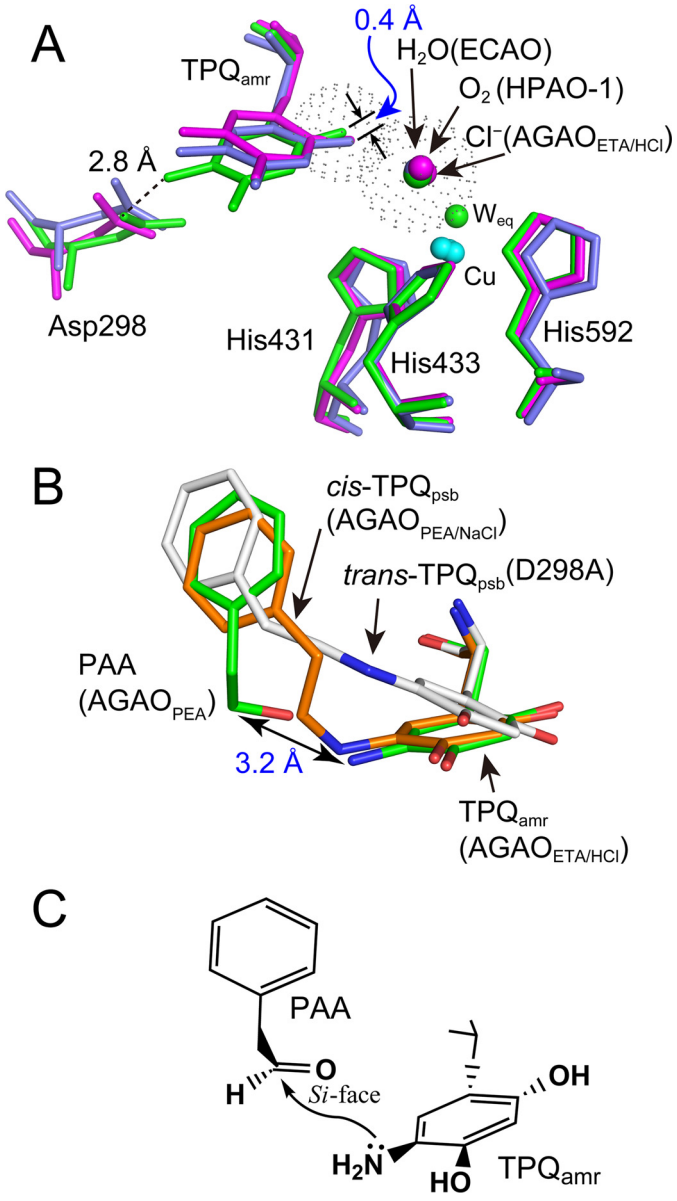

FIGURE 11. **Effect of binding of chloride ion at the axial position of the copper center on the conformation of TPQ_{amr}.** *A*, conformation of the TPQ_{amr} ring in the $AGAO_{ETA/HCl}$ structure (*green*) is compared with those of the substrate-reduced *E. coli* CAO (*ECAO*) (*purple*) and HPAO-1 (*magenta*). *Cyan spheres*, copper atoms. Residue numbers are referred to those of AGAO. van der Waals surfaces of the chloride ion and the oxygen atom of the 2-OH group of TPQ_{amr} are represented with *gray dots*. *B*, comparison of *cis*-TPQ_{psb} formed in $AGAO_{PEA/NaCl}$ (*orange*), *cis*-TPQ_{psb} formed in the D298A mutant of AGAO (29) (*gray*), TPQ_{amr} formed in $AGAO_{ETA/HCl}$ (*green*), and PAA formed in $AGAO_{PEA}$ (*green*). *C*, schematic drawing of the presumed mechanism of the formation of *cis*-TPQ_{psb} in $AGAO_{PEA/NaCl}$.

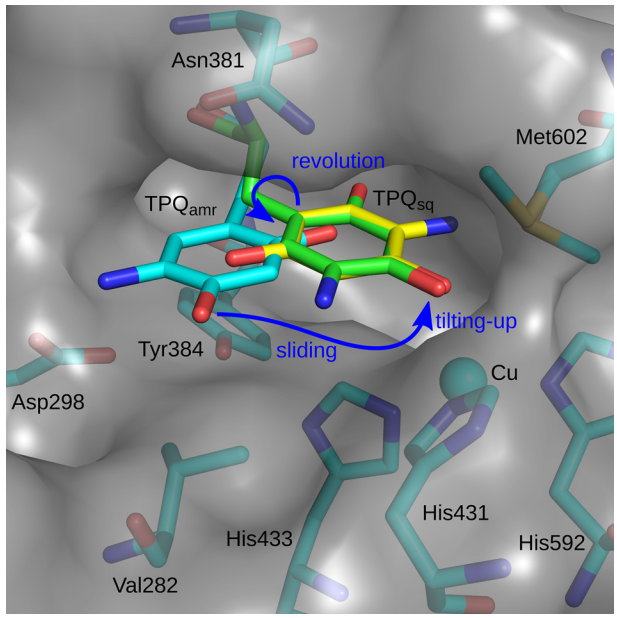

FIGURE 12. **Possible route for the conformational change of TPQ in the active site of AGAO.** *Stick models* of the active-site residues in $AGAO_{ETA/HCl}$ (TPQ_{amr}, *cyan*) and $AGAO_{PEA}$ (TPQ_{sq}, *yellow*) are shown within the cavity with its surface drawn in *half-transparent gray*. The on-copper TPQ_{amr} conformer predicted after the first combined sliding/tilting up motion is *colored green*. The following 180° rotation of the TPQ ring provides a conformation identical with that of the on-copper TPQ_{sq}. The rotation direction and movement of the TPQ ring are shown with *blue arrows*. The figure was generated with PyMOL.

(Fig. 2) by axially coordinating to the copper center (Figs. 7*F* and 8 (*D* and *E*)), whereas azide converts TPQ_{sq} into a ligand-to-metal charge transfer complex (57), and cyanide facilitates TPQ_{sq} formation (61), both of which were suggested to bind at an equatorial position of the copper center (69, 70). It is assumed that azide is probably too large to bind axially to the copper atom and probably cyanide too. Although we cannot currently explain why halide ions, but not azide/cyanide, bind at the axial position of the copper center in the reduced form of TPQ and inhibit TPQ_{sq} formation, it is reasonable to assume that halide ion binding at the axial position of the copper atom would block the coordination of the 4-OH group of TPQ_{amr} to the copper center and prevent the subsequent electron transfer to Cu(II). The inability of halide ions to bind to the axial position of the copper center in the resting TPQ_{ox} state (Fig. 8*F*) may be due to electrostatic repulsion from the delocalized negative charge through the 4-O^- to 2-C=O group of TPQ_{ox}; in the TPQ_{amr} state, both the 2-OH and 4-OH groups (whose estimated pK_a values are 11.62 and 9.59, respectively) (54) are neutral and therefore would not electrostatically repel halide ions. The uncompetitive inhibition of halide ions with respect to the amine substrate is consistent with their binding only to the reaction intermediate, whereas noncompetitive inhibition with respect to dioxygen indicates halide binding at a site distinct from the O_2-binding site. The exclusive binding of halide ions to Cu(II) with TPQ_{amr} in the off-copper conformation (which does not bind dioxygen) is challenging to reconcile with their activity as inhibitors of the oxidative half-reaction that are noncompetitive with respect to dioxygen. This issue can be resolved by supposing that dioxygen binds directly to Cu(I) with TPQ_{sq} in the on-copper conformation during the oxidative half-reaction and undergoes 1 e^--reduction by Cu(I) through the inner sphere mechanism proposed for AGAO (37, 38). Alternatively, halide ions may inhibit the oxidative half-reaction by binding to the O_2-bound enzyme.

The off-copper to on-copper conformational change of TPQ_{amr} involves three motions of the TPQ ring: sliding (~53° rotation around the Cα–Cβ bond), tilting up (~20° rigid body rotation centered at the Cα carbon), and revolution (180° rotation around the Cβ–Cγ bond) (Fig. 12). In the off-copper con-

formation, the TPQ ring is sandwiched between the side chains of Asn-381 and Tyr-384/Val-282 in a narrow wedge-shaped space (29, 53). The initial step of the conformational change is a simultaneous combination of sliding and tilting up in order to avoid a steric clash between the TPQ ring and the side chain of His-433, which would come within ~1 Å of the ring if it only slid. This combined sliding/tilting-up motion leads to the axial coordination of the 4-OH group of TPQ_{amr} to the copper atom, where there is sufficient space for the TPQ ring to rotate by 180° around the Cβ–Cγ bond. The final 180° rotation of the TPQ ring can only occur in the clockwise direction because anti-clockwise rotation would lead to a clash between the 5-NH_2 group and the His-433 side chain while permitting a minor movement of the Tyr-384 side chain (Fig. 12). It is unclear whether the electron transfer from TPQ_{amr} to Cu(II) occurs immediately upon formation of the on-copper conformation of the TPQ ring or after the 180° rotation to the final conformation stabilized by the hydrogen-bonding network (Fig. 9*A*).

Finally, it is noteworthy that the on-copper TPQ_{sq} structure stabilizes the conformation of the side chain of Met-602 by hydrogen bond formation between the 5-NH_2 group of TPQ_{sq} and the Sδ atom of Met-602 (Fig. 9). Met-602 is located at the end of the predicted O_2 pathway from the O_2-prebinding site to the copper center and has conformational flexibility with dual extreme conformers (19). Thus, it is tempting to speculate that the tethering of the Met-602 side chain could act as a gate to allow O_2 to enter into the copper center in the initial phase of the oxidative half-reaction.

In conclusion, the results presented herein show that TPQ undergoes a large conformational change during the reductive half-reaction of AGAO, which efficiently mediates between the acid/base chemistry conducted in the off-copper conformation of TPQ by the conserved catalytic base (Asp-298 in AGAO) and the redox chemistry conducted in the on-copper conformation of TPQ at the metal center.

Author Contributions—T. M., A. H., S. N., T. N., H. Y., K. T., and T. O. participated in research design. T. M., A. H., S. N., M. K., Y. K., and T. O. conducted experiments. All authors performed data analysis and wrote or contributed to the writing of the manuscript.

Acknowledgments—This work was performed using synchrotron beamline stations BL44XU and BL38B1 at SPring-8 under the Cooperative Research Program of the Institute for Protein Research, Osaka University (Proposals 2007A6904, 2007B6904, 2008A6808, 2008B6808, 2009A6911, 2009B6911, 2013A6810, 2013B6810, 2014A6912, and 2014B6912) and with approval from the Japan Synchrotron Radiation Institute (Proposals 2009A1148, 2009B1106, 2010A1203, 2014A1144). The MX225HE CCD detector (Rayonix) at BL44XU was supported by Academia Sinica and the National Synchrotron Radiation Research Center (Taiwan).

References

1. MacIntire, W. S., and Hartmann, C. (1993) in *Principles and Applications of Quinoproteins* (Davidson, V. L., ed) pp. 97–171, Marcel Dekker, New York
2. Floris, G., and Mondovi, B. (eds) (2009) *Copper Amine Oxidases: Structures, Catalytic Mechanisms and Role in Pathophysiology*, CRC Press, Inc., Boca Raton, FL
3. Klema, V. J., and Wilmot, C. M. (2012) The role of protein crystallography in defining the mechanisms of biogenesis and catalysis in copper amine oxidase. *Int. J. Mol. Sci.* **13,** 5375–5405
4. Maintz, L., and Novak, N. (2007) Histamine and histamine intolerance. *Am. J. Clin. Nutr.* **85,** 1185–1196
5. Jalkanen, S., Karikoski, M., Mercier, N., Koskinen, K., Henttinen, T., Elima, K., Salmivirta, K., and Salmi, M. (2007) The oxidase activity of vascular adhesion protein-1 (VAP-1) induces endothelial E- and P-selectins and leukocyte binding. *Blood* **110,** 1864–1870
6. Hernandez, M., Solé, M., Boada, M., and Unzeta, M. (2006) Soluble semicarbazide sensitive amine oxidase (SSAO) catalysis induces apoptosis in vascular smooth muscle cells. *Biochim. Biophys. Acta* **1763,** 164–173
7. Lucero, H. A., and Kagan, H. M. (2006) Lysyl oxidase: an oxidative enzyme and effector of cell function. *Cell Mol. Life Sci.* **63,** 2304–2316
8. Cona, A., Rea, G., Angelini, R., Federico, R., and Tavladoraki, P. (2006) Functions of amine oxidases in plant development and defense. *Trends Plant Sci.* **11,** 80–88
9. Mészáros, Z., Karádi, I., Csányi, A., Szombathy, T., Romics, L., and Magyar, K. (1999) Determination of human serum semicarbazide-sensitive amine oxidase activity: a possible clinical marker of atherosclerosis. *Eur. J. Drug Metab. Pharmacokinet.* **24,** 299–302
10. Yu, P. H., Davis, B. A., and Deng, Y. (2001) 2-Bromoethylamine as a potent selective suicide inhibitor for semicarbazide-sensitive amine oxidase. *Biochem. Pharmacol.* **61,** 741–748
11. Inoue, T., Morita, M., Tojo, T., Nagashima, A., Moritomo, A., and Miyake, H. (2013) Novel 1*H*-imidazol-2-amine derivatives as potent and orally active vascular adhesion protein-1 (VAP-1) inhibitors for diabetic macular edema treatment. *Bioorg. Med. Chem.* **21,** 3873–3881
12. Matsuzaki, R., Fukui, T., Sato, H., Ozaki, Y., and Tanizawa, K. (1994) Generation of the topa quinone cofactor in bacterial monoamine oxidase by cupric ion-dependent autooxidation of a specific tyrosyl residue. *FEBS Lett.* **351,** 360–364
13. Klinman, J. P., and Mu, D. (1994) Quinoenzymes in biology. *Annu. Rev. Biochem.* **63,** 299–344
14. Choi, Y. H., Matsuzaki, R., Fukui, T., Shimizu, E., Yorifuji, T., Sato, H., Ozaki, Y., and Tanizawa, K. (1995) Copper/topa quinone-containing histamine oxidase from *Arthrobacter globiformis.* Molecular cloning and sequencing, overproduction of precursor enzyme, and generation of topa quinone cofactor. *J. Biol. Chem.* **270,** 4712–4720
15. Okajima, T., and Tanizawa, K. (2009) Mechanism of TPQ biogenesis in prokaryotic copper amine oxidase in *Copper Amine Oxidases: Structures, Catalytic Mechanisms and Role in Pathophysiology* (Floris, G., and Mondovi, B., eds) pp. 103–118, CRC Press, Inc., Boca Raton, FL
16. Parsons, M. R., Convery, M. A., Wilmot, C. M., Yadav, K. D., Blakeley, V., Corner, A. S., Phillips, S. E., McPherson, M. J., and Knowles, P. F. (1995) Crystal structure of a quinoenzyme: copper amine oxidase of *Escherichia coli* at 2 Å resolution. *Structure* **3,** 1171–1184
17. Wilce, M. C. J., Dooley, D. M., Freeman, H. C., Guss, J. M., Matsunami, H., McIntire, W. S., Ruggiero, C. E., Tanizawa, K., and Yamaguchi, H. (1997) Crystal structures of the copper-containing amine oxidase from *Arthrobacter globiformis* in the holo and apo forms: implications for the biogenesis of topaquinone. *Biochemistry* **36,** 16116–16133
18. Kishishita, S., Okajima, T., Kim, M., Yamaguchi, H., Hirota, S., Suzuki, S., Kuroda, S., Tanizawa, K., and Mure, M. (2003) Role of copper ion in bacterial copper amine oxidase: spectroscopic and crystallographic studies of metal-substituted enzymes. *J. Am. Chem. Soc.* **125,** 1041–1055
19. Murakawa, T., Hayashi, H., Sunami, T., Kurihara, K., Tamada, T., Kuroki, R., Suzuki, M., Tanizawa, K., and Okajima, T. (2013) High-resolution crystal structure of copper amine oxidase from *Arthrobacter globiformis*: assignment of bound diatomic molecules as O_2. *Acta Crystallogr. D Biol. Crystallogr.* **69,** 2483–2494
20. Li, R., Klinman, J. P., and Mathews, F. S. (1998) Copper amine oxidase from *Hansenula polymorpha*: the crystal structure determined at 2.4 Å resolution reveals the active conformation. *Structure* **6,** 293–307
21. Chang, C. M., Klema, V. J., Johnson, B. J., Mure, M., Klinman, J. P., and Wilmot, C. M. (2010) Kinetic and structural analysis of substrate specificity in two copper amine oxidases from *Hansenula polymorpha*. *Biochemistry* **49,** 2540–2550

22. Duff, A. P., Cohen, A. E., Ellis, P. J., Kuchar, J. A., Langley, D. B., Shepard, E. M., Dooley, D. M., Freeman, H. C., and Guss, J. M. (2003) The crystal structure of *Pichia pastoris* lysyl oxidase. *Biochemistry* **42,** 15148–15157
23. McGrath, A. P., Mithieux, S. M., Collyer, C. A., Bakhuis, J. G., van den Berg, M., Sein, A., Heinz, A., Schmelzer, C., Weiss, A. S., and Guss, J. M. (2011) Structure and activity of *Aspergillus nidulans* copper amine oxidase. *Biochemistry* **50,** 5718–5730
24. Kumar, V., Dooley, D. M., Freeman, H. C., Guss, J. M., Harvey, I., McGuirl, M. A., Wilce, M. C., and Zubak, V. M. (1996) Crystal structure of a eukaryotic (pea seedling) copper-containing amine oxidase at 2.2 Å resolution. *Structure* **4,** 943–955
25. Lunelli, M., Di Paolo, M. L., Biadene, M., Calderone, V., Battistutta, R., Scarpa, M., Rigo, A., and Zanotti, G. (2005) Crystal structure of amine oxidase from bovine serum. *J. Mol. Biol.* **346,** 991–1004
26. McGrath, A. P., Hilmer, K. M., Collyer, C. A., Shepard, E. M., Elmore, B. O., Brown, D. E., Dooley, D. M., and Guss, J. M. (2009) Structure and inhibition of human diamine oxidase. *Biochemistry* **48,** 9810–9822
27. Airenne, T. T., Nymalm, Y., Kidron, H., Smith, D. J., Pihlavisto, M., Salmi, M., Jalkanen, S., Johnson, M. S., and Salminen, T. A. (2005) Crystal structure of the human vascular adhesion protein-1: unique structural features with functional implications. *Protein Sci.* **14,** 1964–1974
28. Jakobsson, E., Nilsson, J., Ogg, D., and Kleywegt, G. J. (2005) Structure of human semicarbazide-sensitive amine oxidase/vascular adhesion protein-1. *Acta Crystallogr. D Biol. Crystallogr.* **61,** 1550–1562
29. Chiu, Y. C., Okajima, T., Murakawa, T., Uchida, M., Taki, M., Hirota, S., Kim, M., Yamaguchi, H., Kawano, Y., Kamiya, N., Kuroda, S., Hayashi, H., Yamamoto, Y., and Tanizawa, K. (2006) Kinetic and structural studies on the catalytic role of the aspartic acid residue conserved in copper amine oxidase. *Biochemistry* **45,** 4105–4120
30. Plastino, J., Green, E. L., Sanders-Loehr, J., and Klinman, J. P. (1999) An unexpected role for the active site base in cofactor orientation and flexibility in the copper amine oxidase from *Hansenula polymorpha*. *Biochemistry* **38,** 8204–8216
31. Murray, J. M., Saysell, C. G., Wilmot, C. M., Tambyrajah, W. S., Jaeger, J., Knowles, P. F., Phillips, S. E., and McPherson, M. J. (1999) The active site base controls cofactor reactivity in *Escherichia coli* amine oxidase: x-ray crystallographic studies with mutational variants. *Biochemistry* **38,** 8217–8227
32. Dooley, D. M., McGuirl, M. A., Brown, D. E., Turowski, P. N., McIntire, W. S., and Knowles, P. F. (1991) A Cu(I)-semiquinone state in substrate-reduced amine oxidases. *Nature* **349,** 262–264
33. Turowski, P. N., McGuirl, M. A., and Dooley, D. M. (1993) Intramolecular electron transfer rate between active-site copper and topa quinone in pea seedling amine oxidase. *J. Biol. Chem.* **268,** 17680–17682
34. Su, Q., and Klinman, J. P. (1998) Probing the mechanism of proton coupled electron transfer to dioxygen: the oxidative half-reaction of bovine serum amine oxidase. *Biochemistry* **37,** 12513–12525
35. Shepard, E. M., and Dooley, D. M. (2006) Intramolecular electron transfer rate between active-site copper and TPQ in *Arthrobacter globiformis* amine oxidase. *J. Biol. Inorg. Chem.* **11,** 1039–1048
36. Welford, R. W., Lam, A., Mirica, L. M., and Klinman, J. P. (2007) Partial conversion of *Hansenula polymorpha* amine oxidase into a "plant" amine oxidase: implications for copper chemistry and mechanism. *Biochemistry* **46,** 10817–10827
37. Shepard, E. M., Okonski, K. M., and Dooley, D. M. (2008) Kinetics and spectroscopic evidence that the Cu(I)-semiquinone intermediate reduces molecular oxygen in the oxidative half-reaction of *Arthrobacter globiformis* amine oxidase. *Biochemistry* **47,** 13907–13920
38. Mukherjee, A., Smirnov, V. V., Lanci, M. P., Brown, D. E., Shepard, E. M., Dooley, D. M., and Roth, J. P. (2008) Inner-sphere mechanism for molecular oxygen reduction catalyzed by copper amine oxidases. *J. Am. Chem. Soc.* **130,** 9459–9473
39. Johnson, B. J., Yukl, E. T., Klema, V. J., Klinman, J. P., and Wilmot, C. M. (2013) Structural snapshots from the oxidative half-reaction of a copper amine oxidase: implications for O_2 activation. *J. Biol. Chem.* **288,** 28409–28417
40. Murakawa, T., Okajima, T., Kuroda, S., Nakamoto, T., Taki, M., Yamamoto, Y., Hayashi, H., and Tanizawa, K. (2006) Quantum mechanical hydrogen tunneling in bacterial copper amine oxidase reaction. *Biochem. Biophys. Res. Commun.* **342,** 414–423
41. Taki, M., Murakawa, T., Nakamoto, T., Uchida, M., Hayashi, H., Tanizawa, K., Yamamoto, Y., and Okajima, T. (2008) Further insight into the mechanism of stereoselective proton abstraction by bacterial copper amine oxidase. *Biochemistry* **47,** 7726–7733
42. Fersht, A. (1998) in *Structure and Mechanism in Protein Science*, pp. 103–131, W. H. Freeman and Co., New York
43. Otwinowski, Z., and Minor, W. (1997) Processing of x-ray diffraction data collected in oscillation mode. *Methods Enzymol.* **276,** 307–326
44. Leslie, A. G. W. (1992) *Joint CCP4 and EESF-EACMB Newsletter on Protein Crystallography*, SERC Daresbury Laboratory, Warrington, UK
45. Collaborative Computational Project, Number 4 (1994) The CCP 4 suite: programs for protein crystallography. *Acta Crystallogr. D Biol. Crystallogr.* **50,** 760–763
46. McCoy, A. J., Grosse-Kunstleve, R. W., Adams, P. D., Winn, M. D., Storoni, L. C., and Read, R. J. (2007) Phaser crystallographic software. *J. Appl. Crystallogr.* **40,** 658–674
47. Murshudov, G. N., Vagin, A. A., and Dodson, E. J. (1997) Refinement of macromolecular structures by the maximum-likelihood method. *Acta Crystallogr. D Biol. Crystallogr.* **53,** 240–255
48. Adams, P. D., Afonine, P. V., Bunkóczi, G., Chen, V. B., Davis, I. W., Echols, N., Headd, J. J., Hung, L.-W., Kapral, G. J., Grosse-Kunstleve, R. W., McCoy, A. J., Moriarty, N. W., Oeffner, R., Read, R. J., Richardson, D. C., Richardson, J. S., Terwilliger, T. C., and Zwart, P. H. (2010) PHENIX: a comprehensive Python-based system for macromolecular structure solution. *Acta Crystallogr. D Biol. Crystallogr.* **66,** 213–221
49. Emsley, P., Lohkamp, B., Scott, W. G., and Cowtan, K. (2010) Features and development of Coot. *Acta Crystallogr. D Biol. Crystallogr.* **66,** 486–501
50. Winn, M. D., Ballard, C. C., Cowtan, K. D., Dodson, E. J., Emsley, P., Evans, P. R., Keegan, R. M., Krissinel, E. B., Leslie, A. G. W., McCoy, A., McNicholas, S. J., Murshudov, G. N., Pannu, N. S., Potterton, E. A., Powell, H. R., Read, R. J., Vagin, A., and Wilson, K. S. (2011) Overview of the *CCP*4 suite and current developments. *Acta Crystallogr. D Biol. Crystallogr.* **67,** 235–242
51. Schüttelkopf, A. W., and van Aalten, D. M. F. (2004) PRODRG: a tool for high-throughput crystallography of protein-ligand complexes. *Acta Crystallogr. D Biol. Crystallogr.* **60,** 1355–1363
52. Ten Eyck, L. F. (1973) Crystallographic fast Fourier transforms. *Acta Crystallogr. A Found. Adv.* **29,** 183–191
53. Murakawa, T., Hayashi, H., Taki, M., Yamamoto, Y., Kawano, Y., Tanizawa, K., and Okajima, T. (2012) Structural insights into the substrate specificity of bacterial copper amine oxidase obtained by using irreversible inhibitors. *J. Biochem.* **151,** 167–178
54. Mure, M., and Klinman, J. P. (1993) Synthesis and spectroscopic characterization of model compounds for the active site cofactor in copper amine oxidase. *J. Am. Chem. Soc.* **115,** 7117–7127
55. Dooley, D. M., McIntire, W. S., McCuirl, M. A., Cote, C. E., and Bates, J. L. (1990) Characterization of the active site of *Arthrobacter* P1 methylamine oxidase: evidence for copper-quinone interactions. *J. Am. Chem. Soc.* **112,** 2782–2789
56. Shimizu, E., Ohta, K., Takayama, S., Kitagaki, Y., Tanizawa, K., and Yorifuji, T. (1997) Purification and properties of phenylethylamine oxidase of *Arthrobacter globiformis*. *Biosci. Biotechnol. Biochem.* **61,** 501–505
57. Juda, G. A., Shepard, E. M., Elmore, B. O., and Dooley, D. M. (2006) A comparative study of the binding and inhibition of four copper-containing amine oxidases by azide: implications for the role of copper during the oxidative half-reaction. *Biochemistry* **45,** 8788–8800
58. Nakatani, H., and Dunford, H. B. (1979) Meaning of diffusion-controlled association rate constants in enzymology. *J. Phys. Chem.* **83,** 2662–2665
59. Masson, P., Lushchekina, S., Schopfer, L. M., and Lockridge, O. (2013) Effects of viscosity and osmotic stress on the reaction of human butyrylcholinesterase with cresyl saligenin phosphate, a toxicant related to aerotoxic syndrome: kinetic and molecular dynamics studies. *Biochem. J.* **454,** 387–399
60. Hardy, L. W., and Kirsch, J. F. (1984) Diffusion-limited component of reactions catalyzed by *Bacillus cereus* β-lactamase I. *Biochemistry* **23,**

1275–1282
61. Shepard, E. M., Juda, G. A., Ling, K. Q., Sayre, L. M., and Dooley, D. M. (2004) Cyanide as a copper and quinone-directed inhibitor of amine oxidases from pea seedlings (*Pisum sativum*) and *Arthrobacter globiformis*: evidence for both copper coordination and cyanohydrin derivatization of the quinone cofactor. *J. Biol. Inorg. Chem.* **9,** 256–268
62. Schwartz, B., Olgin, A. K., and Klinman, J. P. (2001) The role of copper in topa quinone biogenesis and catalysis, as probed by azide inhibition of a copper amine oxidase from yeast. *Biochemistry* **40,** 2954–2963
63. Wilmot, C. M., Hajdu, J., McPherson, M. J., Knowles, P. F., and Phillips, S. E. (1999) Visualization of dioxygen bound to copper during enzyme catalysis. *Science* **286,** 1724–1728
64. Dooley, D. M., Scott, R. A., Knowles, P. F., Colangelo, C. M., McGuirl, M. A., and Brown, D. E. (1998) Structures of the Cu(I) and Cu(II) forms of amine oxidases from x-ray absorption spectroscopy. *J. Am. Chem. Soc.* **120,** 2599–2605
65. Dooley, D. M., and Brown, D. E. (1996) Intramolecular electron transfer in the oxidation of amines by methylamine oxidase from *Arthrobacter* P1. *J. Biol. Inorg. Chem.* **1,** 205–209
66. Kyte, J. (1995) *Mechanism in Protein Chemistry*, pp. 350–371, Garland Publishing, Inc., New York
67. Lopes Jesus, A. J., and Redinha, J. S. (2011) Charge-assisted intramolecular hydrogen bonds in disubstituted cyclohexane derivatives. *J. Phys. Chem. A* **115,** 14069–14077
68. Bisby, R. H., Johnson, S. A., Parker, A. W., and Tavender, S. M. (1999) Time-resolved resonance Raman studies of radicals from 4-aminoresorcinol as models for the active site radical intermediate in copper amine oxidases. *Laser Chem.* **19,** 201–208
69. Dooley, D. M., and Cote, C. E. (1985) Copper(II) coordination chemistry in bovine plasma amine oxidase: azide and thiocyanate binding. *Inorg. Chem.* **24,** 3996–4000
70. McGuirl, M. A., Brown, D. E., and Dooley, D. M. (1997) Cyanide as a copper-directed inhibitor of amine oxidases: implications for the mechanism of amine oxidation. *J. Biol. Inorg. Chem.* **2,** 336–342